Influence of Mg Incorporation on Mechanical, Dielectric and Biological Properties of Hydroxyapatite Ceramic

Alliya Qamar
Lahore College for Women University
Rehana Zia
Lahore College for Women University
Madeeha Riaz (madeehariaz2762@yahoo.com)
College for Women University https://orcid.org/0000-0001-6297-727X
Tousif Hussain
Government College University Lahore
Safia Anjum
Lahore College for Women University

Research Article

Keywords: Calcium Phosphate, Magnesium, Whitlockite, Bioactivity, Dielectric, Hardness

Posted Date: October 28th, 2020

DOI: https://doi.org/10.21203/rs.3.rs-97422/v1

Influence of Mg incorporation on mechanical, dielectric and biological properties of hydroxyapatite ceramic

Alliya Qamar[a], Rehana Zia[a], Madeeha Riaz[a*], Tousif Hussain[b], Safia Anjum[a]

[a]*Physics department, Lahore College for Women University, Lahore, Pakistan*
[b]*Centre for Advanced Studies in Physics (CASP), GCU, Lahore, Pakistan*
Corresponding email: madeehariaz2762@yahoo.com

Abstract

This research focused on the mechanical electrical and biological properties of magnesium doped (Mg_x, x = 0.5 - 2.5 mol%) hydroxyapatite(Hap) using chemical method. It was observed that addition of magnesium produced the secondary phase (whitlockite) depended on the concentration of magnesium using the XRD, FTIR and Raman techniques. These two phases forming BCP(Biphasic) are beneficial from the implant point of view. The dielectric properties were measured as a function of frequency for different concentration of Mg. For 1.0 -2.0mol% doped Mg samples showed dielectric constant value within the range required for implant material. The bioactivity and However, beyond 2mol% of Mg third phase of magnesium oxide was also observed which enhanced the micro-hardness and bioactivity of specimen.

Keywords: Calcium Phosphate; Magnesium; Whitlockite; Bioactivity; Dielectric; Hardness

1. Introduction

Calcium phosphate based bioceramics are suitable as synthetic bone substitutes due to their bioactive and biocompatible that occur in different phases[1]. Hydroxyapatite(Hap) and beta tricalcium phosphate(β-Tcp) are the naturally occurring calcium phosphate bioceramics in bones and teeth of mammals. These two phases makes an exceptional combination for bone implantation with bone-bonding ability of Hap and good bioresorbability of β-Tcp in physiological environment[2, 3] . An optimal ratio of these two can enhance the regeneration of bone in the body environment [4, 5, 6]. It is noteworthy that research is not only concentrated on the biological properties of these ceramics but also electrical and mechanical properties are of great interest. It has been reported that electrical stimulation enhance the growth rate thus reduce the healing time [7, 8]. The electrical response of Hap is analogous to bone[9], thus it is important to study the behavior under the influence of electric field. The crystalline structure(hexagonal) of Hap is quite flexible to accommodate the impurities that in turn can enhance the biological, mechanical and dielectric properties of Hap. According to the previous studies, dielectric properties help in bone regeneration. Little work has been previously done to study dielectric properties for doped calcium phosphate. Magnesium is a vital element in bone formation and its deficiency causes brittleness and bone loss[10, 11]. Thus Mg can be incorporated into Hap structure to augment its properties.

In this study, Mg doped hydroxyapatite was synthesized using wet chemical method. Thermal, Structural, Chemical, mechanical, dielectric and biological properties of undoped and Mg doped samples will be discussed.

2. Materials and Method

All the samples were synthesized by chemical precipitation method[12, 13]. Calcium nitrate, diammonium hydrogen phosphate and Magnesium nitrate were used as a calcium(Ca^{2+}), phosphate and magnesium ions respectively, all of analytical grade. Ammonia solution was used to control the pH. The reaction will take place according to the equaton(1). The schematic for the synthesis is illustrated in Figure 1.

$$(10-x)Ca(NO_3)_2.4H_2O + xMgNO_3 + 6(NH_4)_2HPO_4 \xrightarrow{NH_4OH(pH=10)} Ca_{10-x}Mg_x(PO_4)_6(OH)_2$$
$$x = 0.0 - 2.5mol\% \quad (1)$$

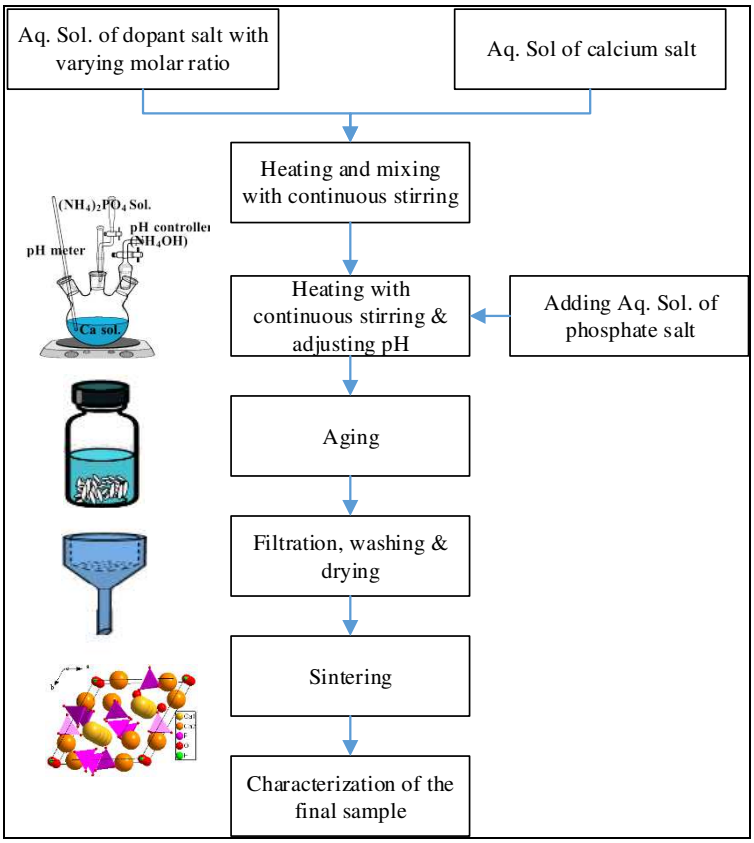

Figure 1 Schematic for Synthesis of the Samples

Solution of calcium and magnesium was prepared with varying concentration (i.e $0 \leq x \leq 2.5$mol% with step size of 0.5mol%) as listed in Table 1. Phosphate solution was added dropwise into Ca/Mg solution with continuous stirring at 80°C for three hours, keeping the pH at 10 using ammonium sol. The samples were kept overnight so that the precipitates settled down, which were then washed thrice with double distilled water. The precipitates were filtered and dried at 90°C. The as-synthesized powders were uniaxially pressed into pellets under 4MPa load. The powders and pellets were then sintered at 1000°C for three hours to get the required samples for analysis.

Table 1 Chemical composition of Mg doped Hydroxyapatite samples

Sample ID	Molar concentration		
	Ca	Mg	P
Mg0.0	10.0	0.0	6
Mg0.5	9.5	0.5	6
Mg1.0	9.0	1.0	6
Mg1.5	8.5	1.5	6
Mg2.0	8.0	2.0	6
Mg2.5	7.5	2.5	6

To determine the thermal characteristics of the samples TGA-DSC (SDT Q600) was used with a heating rate of 10°C/min. The chemical bond characteristics of samples were determined by Midac M2000, recorded in the range of 450 to 4000cm^{-1}. To investigate the effects of incorporation of Mg^{2+} in the structure of the samples Raman spectroscopy(Advantage 532 Raman Spectrometer) was performed. The structure of undoped and Mg-doped samples were characterized using XRD(Bruker D8 Advance X-ray diffractometer) with step size of 0.02 in the 2θ range from 10^o – 80^o . The experimental XRD patterns were identified by comparing them with the standard JCPDS(Joint committee in Powder Diffraction and Standards). Scanning electron microscope(JSM 6480 VL, Joel) was used to study the surface morphology of the samples. The hardness of the samples were determined using Vickers hardness(Suntech Clark Model Cv-700at) with a load of 9.8N applied for 10s on the surface of each compressed polished disc. Dielectric properties were studied by measuring the capacitance and resistance in parallel plate configuration with Precision Impedance Analyzer(Wayne Kerr 6500B) .The bioactivity of the samples was examined by immersing them in Simulated Body Fluid(SBF)[14] solution for two weeks incubated at 37^{o}C under static condition. The antioxidant activity of the samples were studied by measuring the absorbance at 517 nm using UV-VIS spectrophotometer (JEOL JSM-6480 LV).

3. Results and Discussion

3.1 Thermal Analysis

Thermal analysis predicts the phase purity and behavior of the material at high temperature. The DSC curves for the samples are illustrated in Figure 2. The DSC profile for Mg0.0 and Mg0.5 illustrated endothermic reaction up to 440^{o}C associated with the removal of adsorbed water. Minor dips at 480 ^{o}C and 574 ^{o}C can be observed in these two curves which were due to condensation and dehydration of hydro-phosphate(HPO_4^{2-}) group[15]. Intense peaks appeared at 956^{o}C(T_2) which are attributed to crystallization of Hap[16]. The peaks at 480^{o}C and 574^{o}C

disappeared in Mg1.0 – Mg2.5, but there was onset of other intense peaks at 856°C(T_1) along with the peaks at T_2. The endothermic peaks at T_1 are attributed to the formation of low temperature Tcp[17]. For Mg2.5 profile curve an endothermic peak at 795°C appeared which might be due to the formation of MgO. Hence, with the addition of Mg formation of β-Tcp occurred and higher conc. of Mg introduces the MgO phase also.

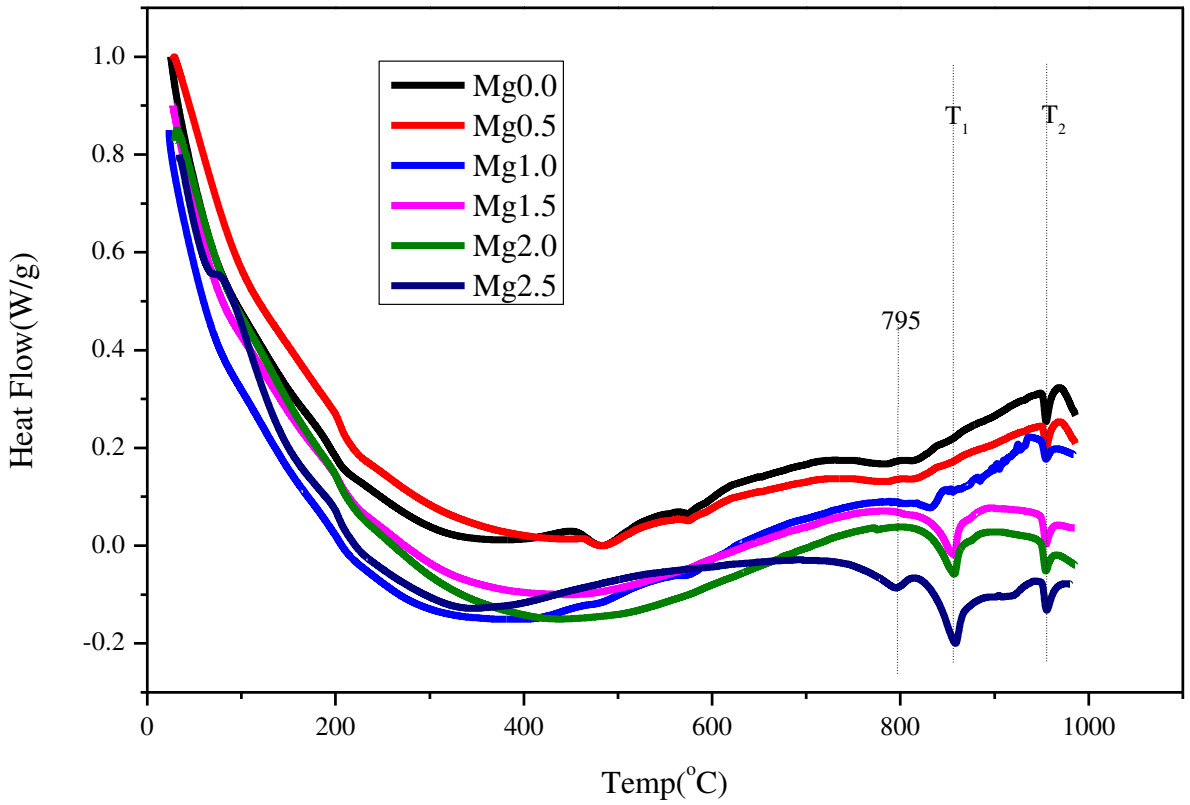

Figure 2 –DSC curves for undoped and Mg-doped samples

3.2 IR Spectra

Several vibrational bands were observed in IR spectra of pure and Mg doped samples as shown in Figure 3. For undoped sample, Mg0.0, the band at 1023(v_1) cm^{-1} and 969(v_2) cm^{-1} correspond to PO_4 stretching band while PO_4 bending bands relate to 605(v_4) and 562(v_4) cm^{-1} that are characteristics of hydroxyapatite[18]. For Mg(1.0 – 2.5mol%) doped samples the IR spectra showed a new band at 1118cm^{-1} which correspond to characteristic β-TCP along with hydroxyapatite characteristic bands[19], listed in Table 2. It was observed that with Mg doping the broadness of vibrational bands were reduced which indicates alignment of atoms.

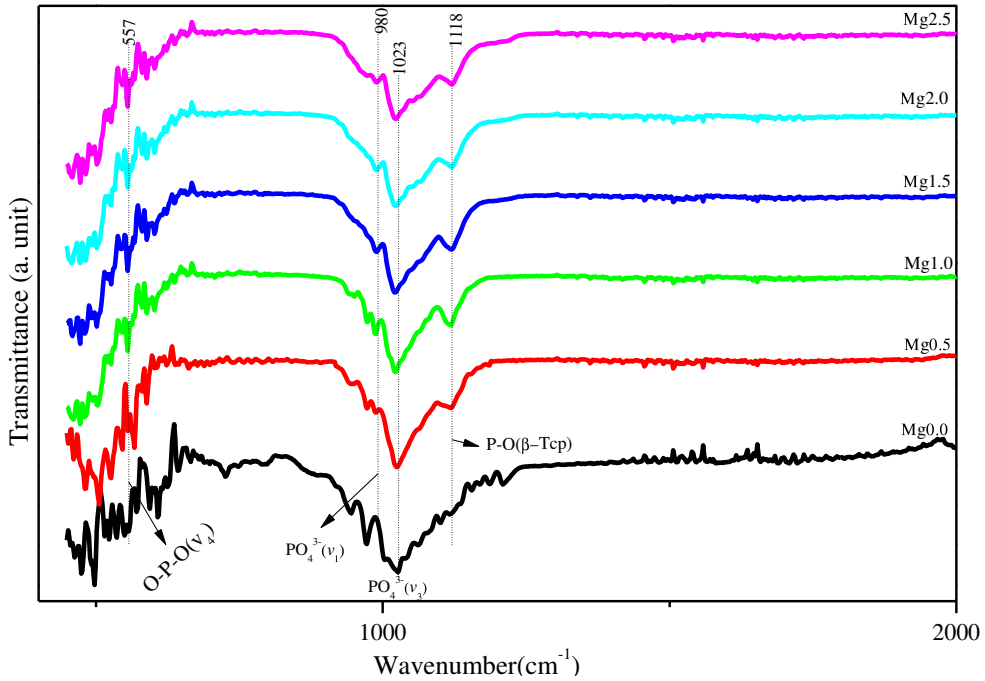

Figure 3 FTIR spectra of undoped and Mg doped hydroxyapatite

Table 2 FTIR band assignments for Mg doped Hydroxyapatite

Wavenumber(cm^{-1})							**Mode**
Mg0.0	**Mg0.5**	**Mg1.0**	**Mg1.5**	**Mg2.0**	**Mg2.5**	**Ref[13, 14, 20 , 21]**	
-	1118	1118	1118	1118	1118	1118	Stretching mode of P-O (TCP)
1023	1023	1023	1023	1023	1023	1029	Asymmetric P-O stretching mode
969.8	977.8	984.3	984.3	984.3	990.1	960-970	Symmetric P-O stretching mode
601.8	601.8	601.8	601.8	601.8	601.8	600-610	O-P-O bending mode/crystal
562	562	562	562	562	562	560-600	O-P-O bending mode/amorphous

3.3 Raman Spectra

The Raman spectra of undoped and Mg doped samples is shown in Figure 4. In all samples hydroxyapatite was prominent by a very robust band at 961cm^{-1} and within 400cm^{-1} (v_2) range of Hap that ascends from the symmetric stretching mode(v_1) of PO_4 group. Other Raman-active band for PO_4 could be seen at 1036cm^{-1}(v_3)[22, 23]. With the addition of 0.5mol% of Mg the distinct peak at 961cm^{-1} splits into double peaks, 948cm^{-1} and 964cm^{-1}, which are attributed to PO_4 stretching mode of β-TCP[24, 25]. Another difference observed was the disappearance of 1036cm^{-1} peak(stretching mode P-O) with addition of Mg up to 1.0mol%. With further addition

of Mg(1.5 – 2.5 mol%) the double peaks at 948cm^{-1} and 946 cm^{-1} combined into a single intense peak. The reappearance of peak corresponding to phosphate vibration at 1051cm^{-1} was observed.

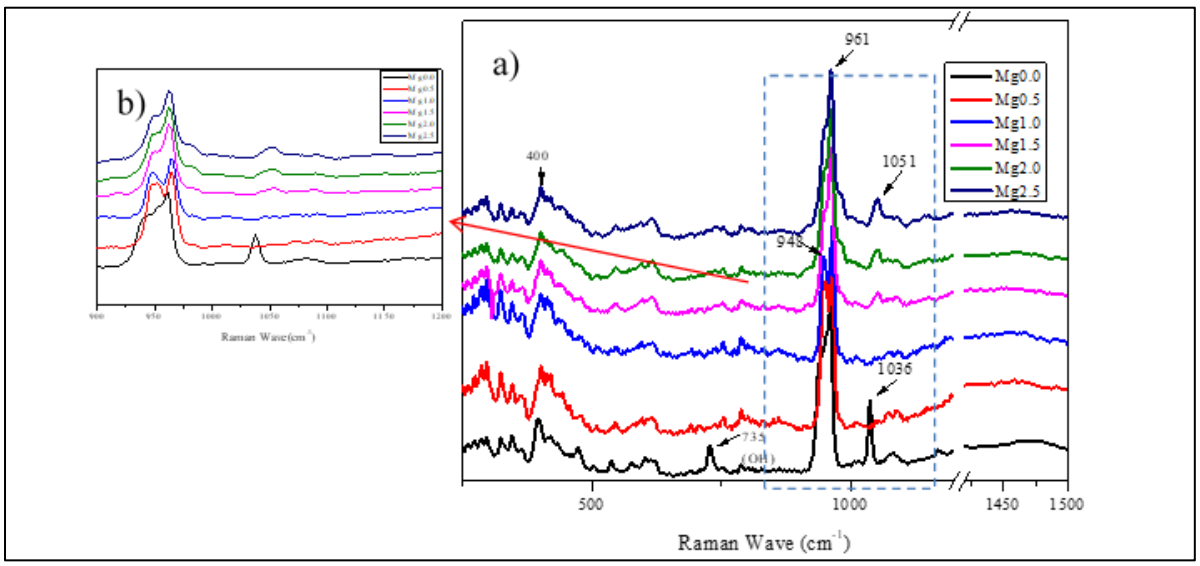

Figure 4 a)Raman Spectra of undoped and Mg doped samples b) Magnified view of a)

3.4 XRD Analysis

X-ray diffraction data was used to determine the lattice parameters, phase analyses and crystallite size of the samples. Figure 5 showed the XRD pattern of Mg substituted hydroxyapatite. Undoped sample Mg0.0 showed single phase hexagonal hydroxyapatite(JCPDS # 09-0432) with peak reflections identified at (002), (102), (210), (211), (112), (300), (202), (310), (311), (302), (222), (213), (312), (320), (004), (331) (hkl) values. This is also justified with IR- spectra and Raman spectra for this sample. With the addition of small amount of Mg0.5(0.5mol%) broadness of the main peaks((211), (112), (300)) could be observed, which corroborates the incorporation of Mg into the Hap due to smaller radius of Mg as compared to Ca[26] also new peaks appeared at 17.08^{o} and 26.7^{o} that correspond to secondary phase. This secondary phase was identified as Mg- β-TCP(whitlockite, JCPDS #1-070-2064). For Mg1.0(1.0mol%) more peaks reflections at 34.63^{o} and 47.36^{o} along with 17.08^{o} and 26.7^{o} of secondary phase were observed. It had been previously reported by P.kanchana and Salami[27, 28] that Mg addition lead to the development of Mg-β-TCP(whitlockite). The presence of the secondary phase was also observed in DSC curves (Figure 2), that showed the exothermic peaks at lower temperature(T_1). Further doping of Mg(1.5-2mol%) new peak reflection at 28.0^{o} , 35.8^{o} and 36.4^{o} of whitlockite phase emerged while peak intensity at 17.3^{o} reduced with Mg addition. For sample Mg2.5 a third phase MgO(JCPDS # 45-946) appeared due to higher concentration of Mg which also compliment the DSC curve for this sample showing a peak at 795^{o}C.

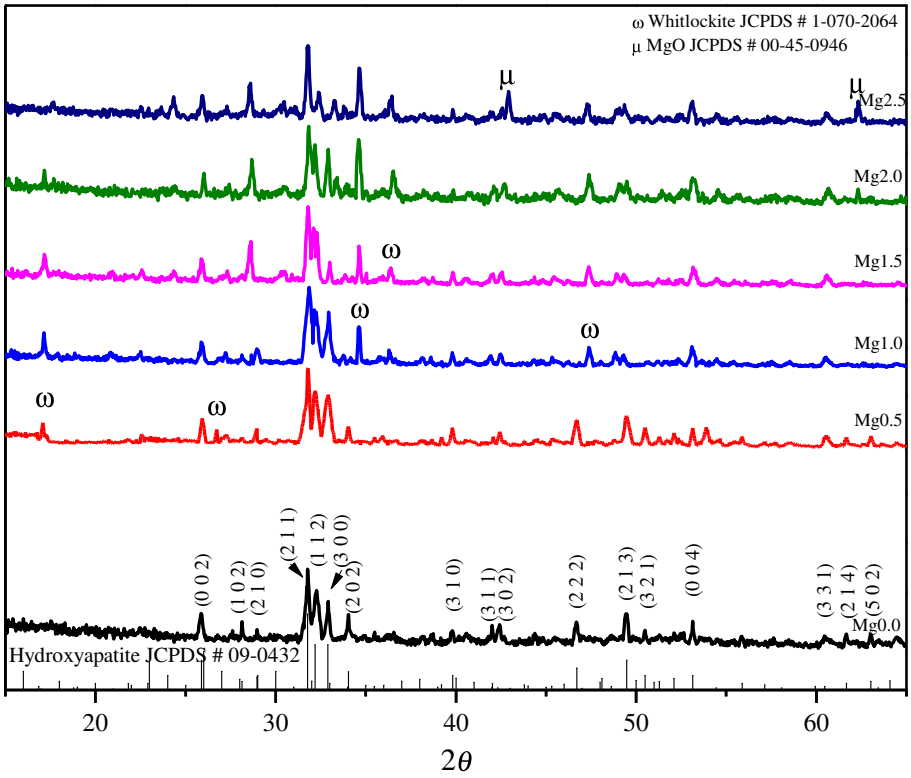

Figure 5 XRD pattern of undoped and Mg(0 – 2.5mol%)

The phase percentage of undoped and Mg-doped samples is listed in Table 3. With the addition of Mg the secondary phase whitlockite /appeared whose percentage is Mg concentration dependent.

Table 3 Phase percentage for undoped and Mg doped Samples

Sample ID	Phase %		
	Hap	β-TCPMg (whitlockite)	MgO
Mg0.0	100%	0%	0%
Mg0.5	89%	11%	0%
Mg1.0	73%	27%	2%
Mg1.5	68%	32%	2%
Mg2.0	63%	37%	2%
Mg2.5	60%	30%	10%

The lattice parameters(*a, c*) and volume(*V*) of the hydroxyapatite were evaluated using the following equations[29]

$$\frac{1}{d^2} = \frac{4}{3}\left(\frac{h^2+hk+k^2}{a^2}\right) + \frac{l^2}{c^2} \quad (1)$$

$$V = a^2 c\, sin(60) \quad (2)$$

Where *d* is interplaner distance and *hkl* are Miller indices. The crystallite size(*D*) and crystallinity percent was calculated using the following relations[30]

$$D = \frac{0.9\lambda}{\beta_{hkl}\cos(\theta_{hkl})} \quad (3)$$

$$X_c = \left(\frac{K}{\beta_{hkl}}\right)^3 \quad (4)$$

The lattice parameters(*a*, *c*) decreased with the increase in concentration of Mg as listed in Table 4 and Table 5, thus suggested the substitution of Mg ion for Ca ion Since Mg ion radius is smaller than Ca ion radius; substitution of Mg ion for Ca ion produced the decrease in the lattice parameters[31, 32]. Substitution of Mg ion for Ca ion produces destabilization/decomposition of the structure. The crystallites became smaller, more irregular and form agglomerates when Mg was substituted [33].

The crystallite size was found to increase for Mg 2.5mol% due to increase of the lattice disorder as a result of the presence of Mg ions and formation of MgO due to surplus Mg.

Table 4 Lattice parameter and volume of the samples as a function of Mg content

Sample ID	***a*[Å]**	***c*[Å]**	***c/a***	***Volume* V[Å]^3**
Mg0.0	9.3960	6.8538	0.7294	524.0226
Mg0.5	9.3795	6.8409	0.7293	521.2002
Mg1.0	9.2987	6.8374	0.7353	511.9902
Mg1.5	9.2792	6.8293	0.7360	509.2523
Mg2.0	9.2786	6.8342	0.7366	509.5431
Mg2.5	9.2407	6.8356	0.7397	505.4936

The value of lattice parameters reduced with the addition of Mg^{2+} for Mg^{2+} 0.5 – 1.5 mol% that confirmed the incorporation of Mg into the lattice. For Mg^{2+} 2.0 – 2.5mol% the value of '***c***' slightly increased identifying the appearance of third phase that caused the lattice disorder and strain. However, the volume decreased due to smaller bond length of Mg^{2+} with O^{2-} as compared to Ca^{2+}.

Table 5 Crystallite Size and Crystallinity of the samples

Sample ID	***Crystallite size D(nm)***	***Crystallinity X_C (%)***
Mg0.0	35.7698	100%

Mg0.5	33.4429	93%
Mg1.0	30.9674	85%
Mg1.5	29.7823	72%
Mg2.0	25.9713	64%
Mg2.5	29.3282	59%

The crystallite size and crystallinity of the samples showed the decreasing trend with the addition of Mg^{2+} (0.5 -2.0mol%) which agreed well with the previous Raman analysis. But for Mg2.5 sample the crystallite size and crystallinity increased this mighty be due to the formation of MgO that reduced the availability of Mg^{2+} for replacement of Ca^{2+} in Hap. The XRD peak intensity at 17.08^{o} for Mg2.5 decreased due to non-availability of Mg^{2+} hence Mg-β-Tcp formation also reduced.

3.5 SEM

SEM micrographs as shown in Figure 6 illustrates the morphology of sintered undoped and Mg-doped samples.

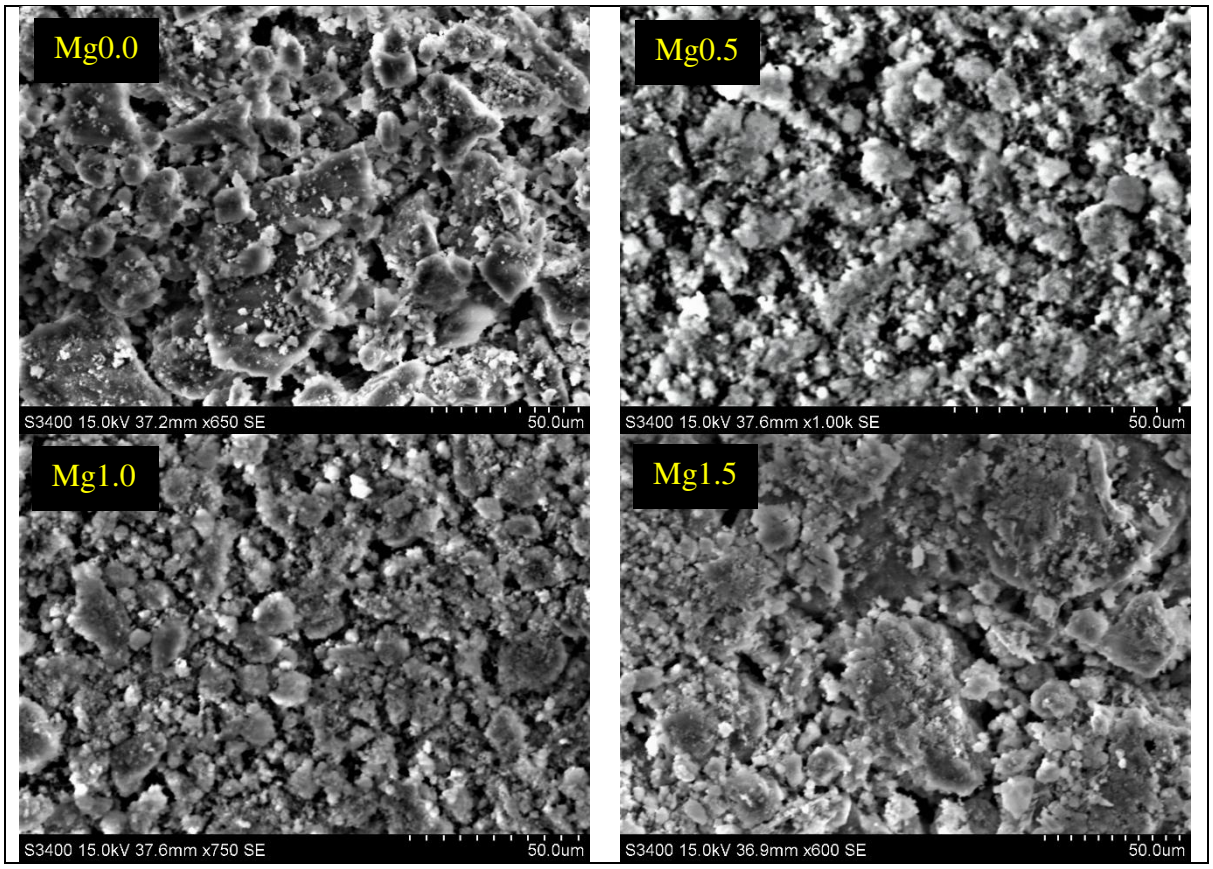

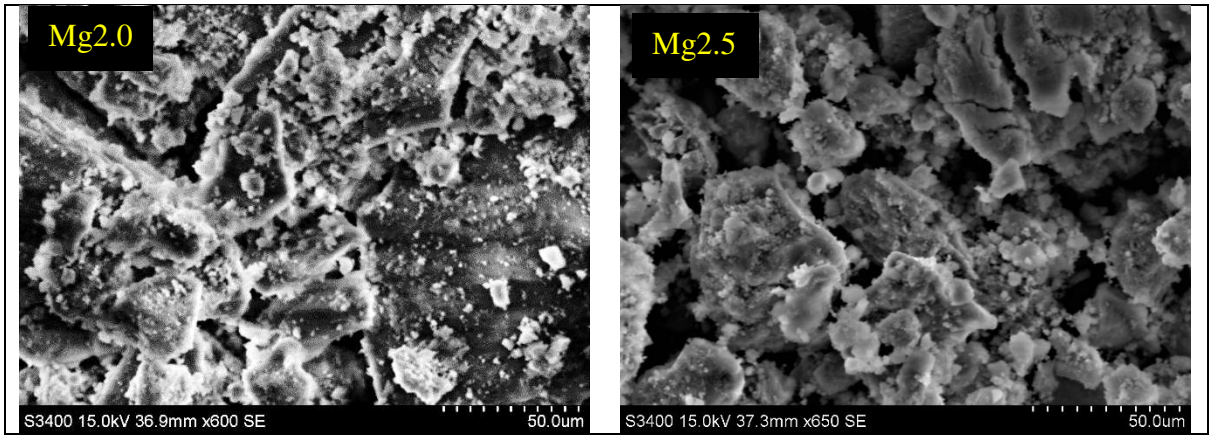

Figure 6 SEM micrograph of Mg doped samples

It can be seen that undoped Hap(Mg0.0) is in form of small-size crystal, by increasing the Mg^{2+} concentration, the densification of particles increases. This densification reduces the elongation and widening of particles so the grain size reduces gradually. After the addition of Mg, these particles have plate like or flakes like morphology. The results of researches indicate that by increasing Mg concentration in Hap, secondary phase (whitlockite) formed so the morphology also varies.

3.6 Mechanical Analysis

The microhardness of the samples was measured using Vickers hardness method. The Vickers hardness was measured using the following formula[34]

$$H = 1.854\frac{F}{d^2} \qquad (5)$$

where F is the load applied and d is mean diameter of the indent. Average value was taken from five indents on each sample. It was observed that the hardness of the doped samples was higher than the undoped samples as shown in Figure 7, having the highest indentation hardness value of 1.01GPa as listed in Table 7. The values are comparable to the human bone ~0.3-0.9 GPa[35]. Since Mg is smaller in size as compared to Ca, the replacement of Ca by Mg would reduce the bond length and increase the bond strength with the O. The upsurge bond strength would be the cause of higher value of microhardnes. Thus the hardness depends on the hydroxyapaptite/ Mg-TCP ratio.

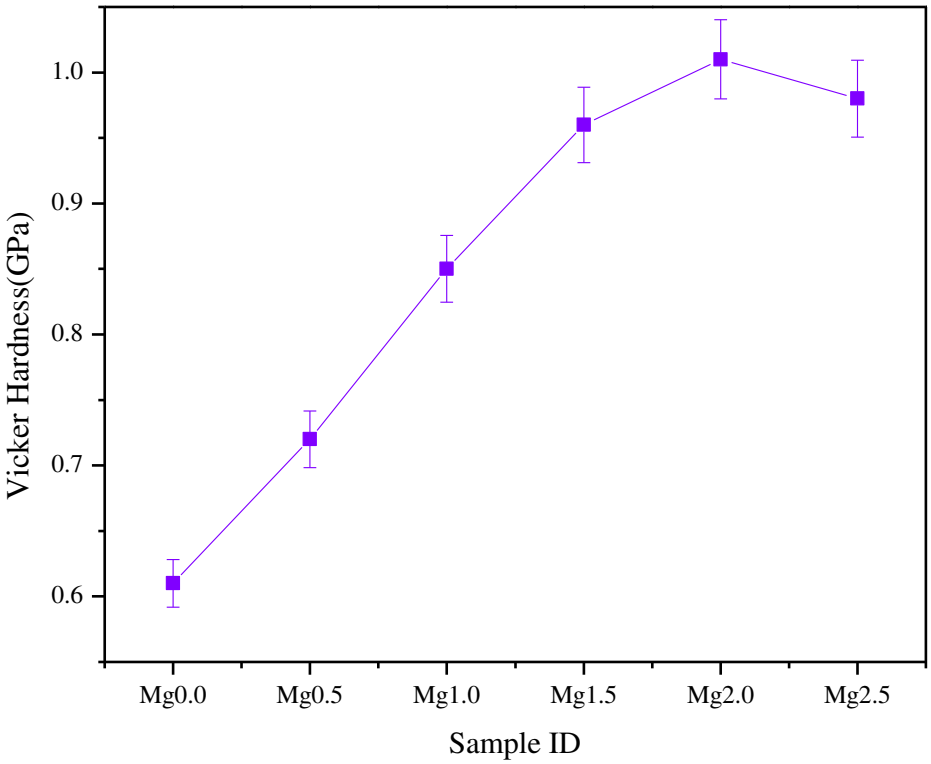

Figure 7 Vicker hardness of undoped and Mg doped samples

Table 7 Hardness of the samples

Sample ID	Hardness(GPa)
Mg0.0	0.61±0.02
Mg0.5	0.72±0.03
Mg1.0	0.85±0.02
Mg1.5	0.96±0.04
Mg2.0	1.01±0.03
Mg2.5	0.98±0.03

The optimal ratio was observed for the Mg content at 2.0mol%, after which the trend showed the decline. The increase in hardness for Mg2.0 sample is due to the appearance of the third phase MgO that enhances the hardness as reported by Satoshi [36]

3.7 Dielectric Properties

The dielectric properties of the implant are of interest in order to augment the bone growth. The dielectric properties of the samples were studied as a function of frequency. The capacitance values were used to calculate the dielectric constant(ε). The dielectric constant, alternating current conductivity (σ_{ac}) and dielectric loss(tan(δ)) were determined using the following formula[37]

$$C_p = \frac{\varepsilon_o \varepsilon A}{t} \quad (6)$$

$$\sigma_{ac} = \frac{t}{ZA} \quad (7)$$

$$\tan(\delta) = \frac{1}{2\pi f C_p R_p} \quad (8)$$

Where C_p is the capacitance, ε_o the free space dielectric constant (8.854×10^{-12} F/m), A is the area, t is the thickness and Z is the impedance of the dielectric samples. The dielectric constant determines the efficiency of the material to store energy(electrical). It is a frequency dependent variable and decreases as the frequency increases.

The dielectric properties of the samples were studied by measuring resistance and capacitance using Impedance Analyzer at room temperature. Figure 8a showed the dielectric constant as a function of frequency from 1KHz to 1MHz. The values of dielectric constant varied as the concentration of dopant varies. It has been observed that the value of ε increases as the conc. of Mg_x increase from $0 \leq x \leq 1.5$ mol% after which it showed the decreasing trend. The dielectric constant decreased as the frequency increased for all the samples. Since the applied electric field produced polarization in the material, as the frequency increased the dielectric constant decreased which is attributed to the failure of the dipoles to follow the alternating electric field frequency and lag behind the applied frequency[38]. The alternating current conductivity increased with the increase in frequency as shown in Figure 8(b), which is attributed either due to H^+ ion bouncing between O^{2-} or OH^{-1} ions with PO_4 group.

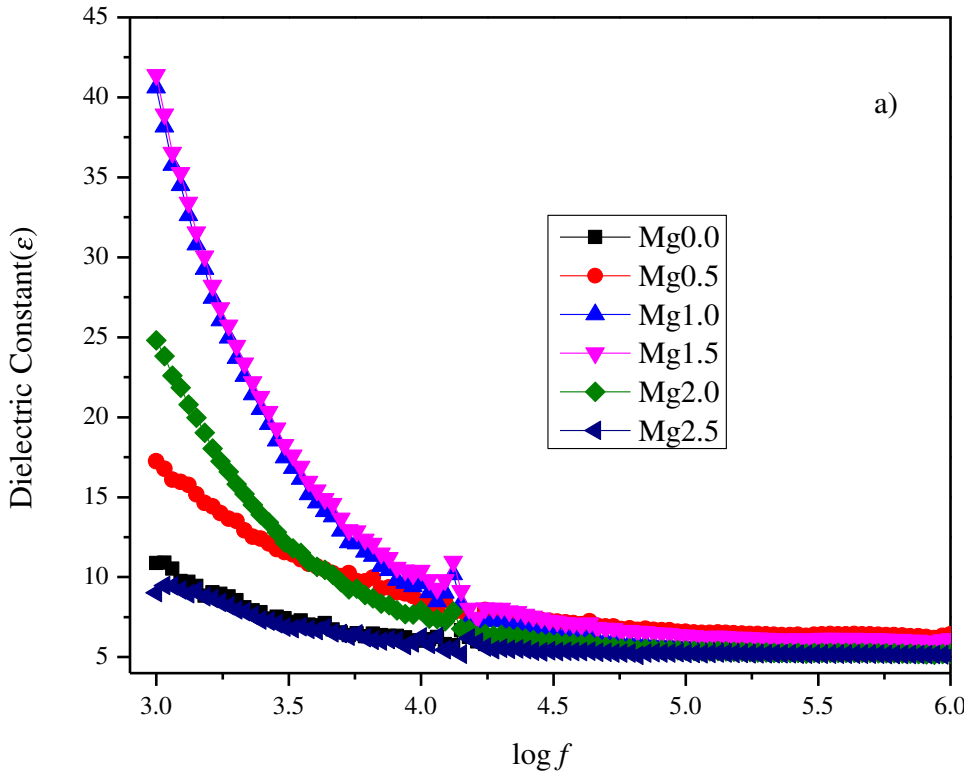

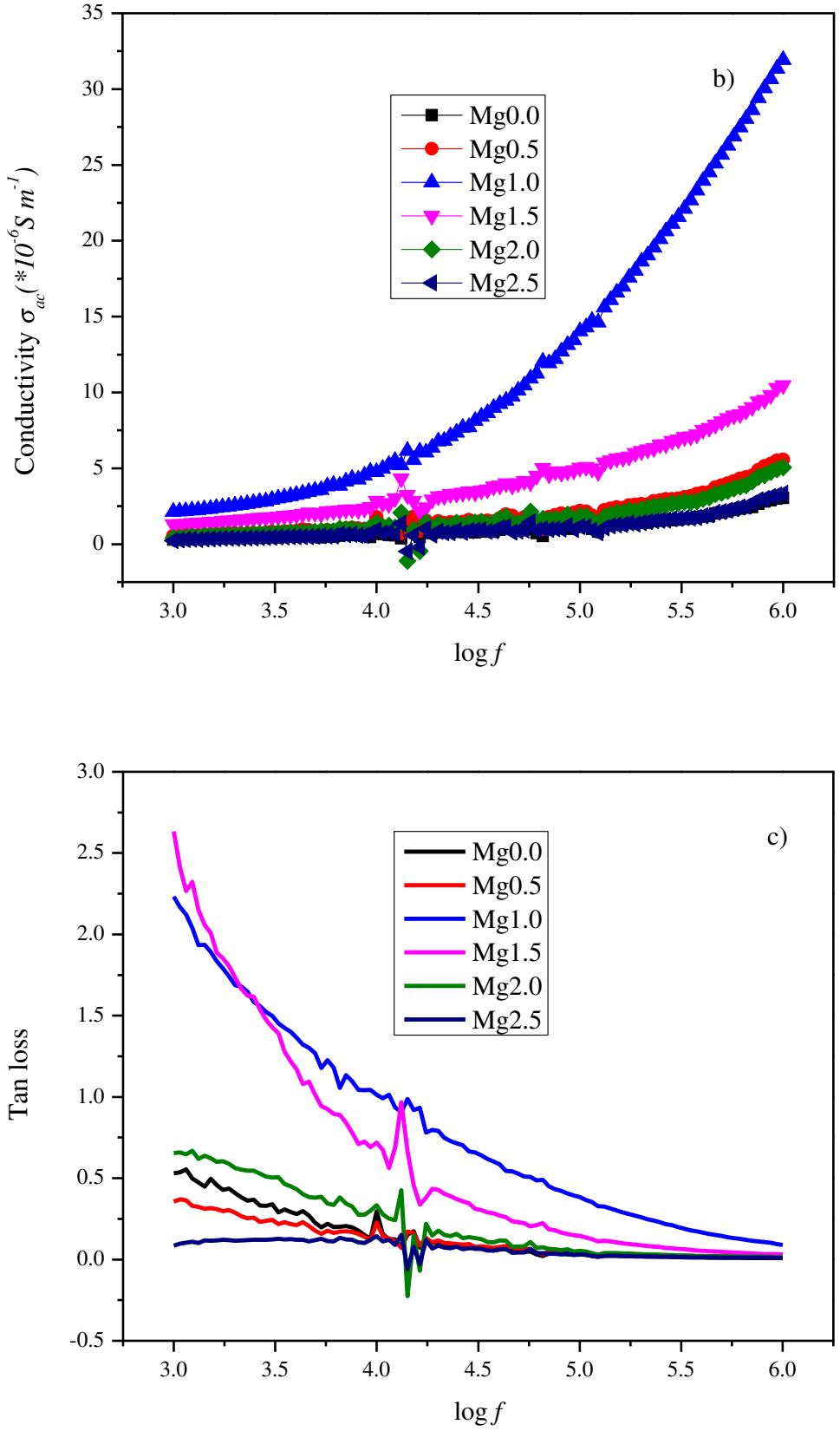

Figure 8 Relative Permativity, AC conductivity and Tangent Loss as a function of frequency for Mg_x content ($0 \leq x \leq 2.5$ mol%).

Tangent loss, absorption of electrical energy by the material, also showed(Figure 8c) the same trend as of dielectric constant and conductivity. The high value of tangent loss for Mg1.0 and Mg1.5 at low frequency are attributed due to defects/impurities present in the samples. All the curves exhibited bulge around 13kHz that is attributed to the resonance between the ions frequency and the frequency of applied field. Thus these results suggest that Hap samples can also be used as dielectric material in biosensors and as a dielectric material in electronic devices.

3.8 Bioactivity

Simulated body fluid(SBF) solution, prepared by Kokubo method [39] was used to assess the bioactivity of the samples. The samples were immersed in SBF solution for two weeks at 37°C, the pH and the concentration of Ca, P and Mg ions in the solution were recorded periodically as shown in Figure 9. Initially there was rise in pH due to release of cations(Ca^{2+}) from the samples this was justified as there was increase in Ca concentration as shown in Figure 9(d) and 9(a) respectively. After four days the pH and Ca concentration started to decrease as the leakage of Ca ions reduced which is attributed to the formation of apatite layer.

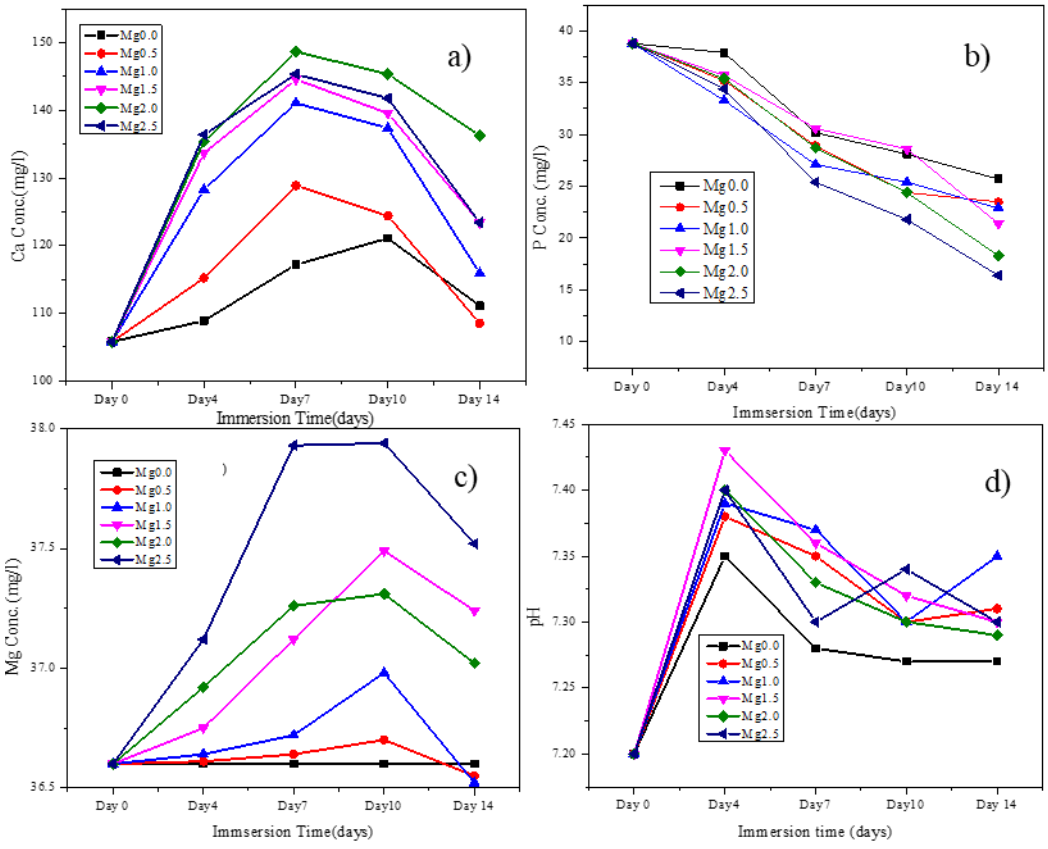

Figure 9 Ca Concentration(a), P concentration(b) Mg concentration(c) and Variation of pH(d) in SBF Sol. For 14 days

The formation of apatite layer in physiological environment depends on the resorbability, which increases the pH. From Figure 9(d) it can be observed that the pH of Mg0.0(undoped) was lower as compared to doped samples the same trend can be seen for Ca and P content. The maximum bioresorbalility was observed for Mg1.5, which is a mixture of Hap and whitlockite having greater percentage of whitlockite phase as compared to the other sample.

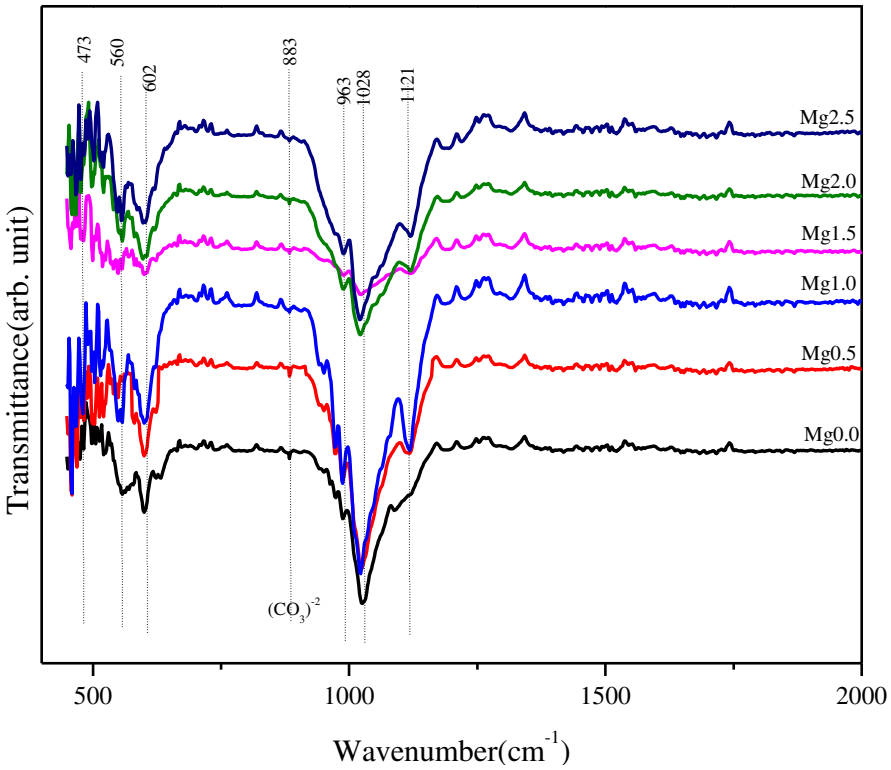

Figure 10 FTIR of undoped and Mg-doped samples after immersion in SBF Sol.

The FTIR spectra of the samples after soaking in SBF-solution for 14 days is shown in Figure 10. The same trend can be seen from the figure as was the case of when the samples were not immersed(Figure 3). However some band become clear and prominent like the bands at 500 - 560cm^{-1} which are due to bending vibration mode(crystalline) of P-O bonds in PO_4^{3-} group[40, 41] and the band around 470 cm $^{-}$1 correspond to double degenerated bending mode(v_2). These bands identify the Hap. It can be observed that the widening of the main broad band centered at 1028cm^{-1} did not occurred for the immersed samples in FTIR transmittance spectrum as compared to the un-immersed. In case of un-immersed samples, the widening occurred due to Mg^{2+} that increased with increasing concentration of Mg^{2+}. The band in the around 1121cm^{-1} related to β-Tcp vibrational mode. Thus, the FTIR analysis showed that the apatite layer formed on the samples were of biological Hap due to appearance of carbonate group.

3.9 Antioxidant Activity

Free radicals produce during oxidation chain reaction that can damage cells. Cell metabolism, ecological pollutants and infective toxins through these oxidative stress exhibit toxic effects[42]. The scavenging of free radicals by antioxidant control the deterioration of the cells. the prevention of many chronic diseases, such as cancer, diabetes and cardiovascular disease, has been suggested to be associated with the antioxidant activity DPPH(2,2-diphenyl-1-picrylhydrazyl) radical scavenging assays were used to determine the radical scavenging effect of the samples. The absorbance was measured at 517 nm and the percentage scavenging activity of radicals was calculated using the formula

$$\% \text{ Scavenging activity} = \frac{(\text{Absorbance of control} - \text{Absorbance of sample})}{\text{Absorbance of control}} \times 100$$

Ascorbic acid was used as standard antioxidant. The antioxidant behavior of hydroxyapatite material was assessed for undoped and Mg doped samples at 15mg/ml concentration as shown in Figure 11

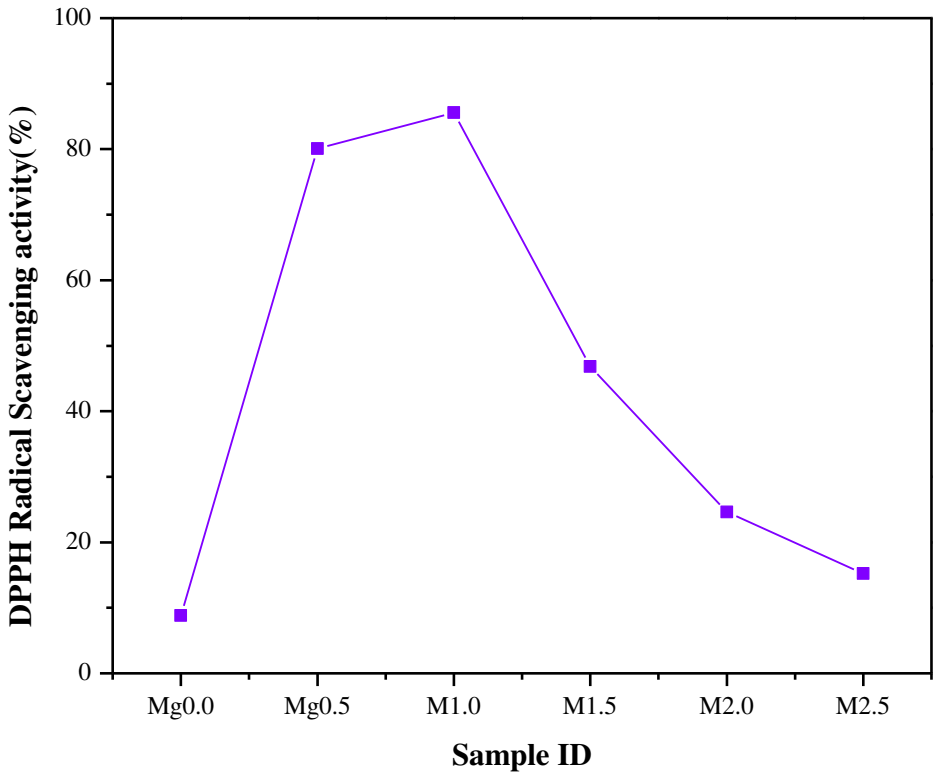

Figure 11 Antioxidant activity of samples for Mg_x content ($0 \leq x \leq 2.5$ mol%).

Scavenging of free radicals increased with doping as compared to the undoped sample. The antioxidant property of Hap could be beneficial for orthopedic and dental implant.

4 Conclusion

Pristine and Mg doped hydroxyapatite were synthesized using chemical method. Incorporation of Magnesium subvert the Hap crystal structure with the formation of whitlockite which was confirmed by XRD, FTIR and Raman spectroscopy. These results illustrated the phase formation, Mg ions substitution in hydroxyapatite and transformation of Hap into other phases with the increase in Mg content. The effects of Mg were linked to the variation of lattice parameters and crystallinity of Hap. Beginning from pristine Hap with regular incorporation of Mg, admixture of the two phase was obtained. However, as the amount of Mg exceeded 2mol% new phase (MgO) appeared due to excess of magnesium. These phases favored the hardness and bioactivity, and for Mg 1.5mol% gave the better result as compared to others. It is possible to obtain the particular ratio of Hap and whitlockite by controlling the Mg concentration during synthesis. The dielectric properties were also affected by the addition of Mg. For 1.0 - 2.0mol% of Mg the dielectric constant value is within the range required for implant material(18 – 68[43]) at lower frequency range. The loss factor of all the samples were at 13kHz. The AC conductivity increased at higher frequency obeying the Jonsher's power law. Scavenging of free radicals increased with doping as compared to the undoped sample. These outcomes could be useful for implant material under the influence of electric field, as well as for biosensor.

Reference:

1. Jiwoon Jeong, Jung Hun Kim, Jung Hee Shim, Nathaniel S. Hwang, Chan Yeong Heo. Bioactive calcium phosphate materials and applications in bone regeneration, *Biomaterials Research* **23**(4) : 1- 11 (2019)

2. Hiroyuki Shibata, Taishi Yokoi, Tomoyo Goto, Ill Yong Kim, Masakazu Kawashita, Koichi Kikuta, Chikara Ohtsuki. Behavior of hydroxyapatite crystals in a simulated body fluid: effects of crystal face, *Journal of the Ceramic Society of Japan* **121**(19) 807-812 (2013)

3. A. Tahmasebifar and Z. Evis. Structural and mechanical characteristics of hydroxyapatite and tri-calcium phosphates doped with Al3+ and F- ions, *Journal of Ceramic Processing Research* **14**(4) : 549 -556 (2013)

4. R. Z. LeGeros, S. Lin, R. Rohanizadeh, D. Mijares, J. P. LeGeros. Biphasic calcium phosphate bioceramics: preparation, properties and applications, *Journal of Materials Science: Materials in Medicine.* **14**(3): 201–209 (2003)

5. J.M. Bouler a, P. Pilet b, O. Gauthier b,c, E. Verron. Biphasic calcium phosphate ceramics for bone reconstruction: A review of biological response, *Acta Biomaterialia* **53 :**1–12 (2017)

6. Hongquan Zhang, Chunpeng Zhao, Jin Wen, Xiaoyan Li, Luwei Fu. Synthesis And Structural Characteristics Of Magnesium And Zinc Doped Hydroxyapatite Whiskers, *Ceramics-Silikaty* **61** (3): 244-249 (2017)

7. Paul RT Kuzyk, Emil H Schemitsch, The science of electrical stimulation therapy for fracture healing, Indian J. of Orthopaedics 43(2) 127-131 (2009)

8. L. Leppik, H. Zhihua, S. Mobini, V. Thottak k., Parameswaran, M. Eischen, A. Slavici, J. Helbing, L. Pindur, K. M. C. Oliveira, M. B. Bhavsar, L. Hudak, D. Henrich, J. H. Barker, Combining electrical stimulation and tissue engineering to treat large bone defects in a rat model, Scientific Reports | (2018) 8:6307

9. B. V. Jogiyaa, H. O. Jethava, K. P. Tank, V. R. Raviya and M. J. Joshi, Impedance and Modulus Spectroscopic Study of nano Hydroxyapatite, AIP Conference Proceedings 1728, 020227 (2016)

10. Sharifah Adzila1, Nanthini Kanasan1, Mohd Fahrul Hassan, Ahmad Mubarak Tajul Arifin, Muhamad Zaini Yunos1, Mohd Nasrull Abdol Rahman, Reazul Haq Abdul Haq. synthesis and characterization of magnesium doped calcium phosphate for bone implant application, *Arpn Journal of engineering and applied sciences* **11** (14) :(2016)

11. K. Thanigai Arul, Elayaraja Kolanthai, E. Manikandan, G.M. Bhalerao V. Sarath Chandra, J. Ramana Ramya , U. Kamachi Mudali , K.G.M. Nair, S.Narayana Kalkura. Green synthesis of magnesium ion incorporated nanocrystalline hydroxyapatite and their

mechanical, dielectric and photoluminescence properties, *Materials Research Bulletin* **67** : 55–62 (2015)

12. S. Gomes, G. Renaudin, A. Mesbah, E. Jallot, C. Bonhomme, F. Babonneau, J.-M. Nedelec. Thorough analysis of silicon substitution in biphasic calcium Phosphate bioceramics: A multi-technique study, *Acta Biomaterialia* **6** : 3264–3274 (2010)

13. Chandra VS1, Baskar G, Suganthi RV, Elayaraja K, Joshy MI, Beaula WS, Mythili R, Venkatraman G, Kalkura SN. Blood Compatibility Of Iron-Doped Nanosized Hydroxyapatite And Its Drug Release, *Appl Mater Interfaces* **4**(3):1200-1210. (2012)

14. Yann C. Fredholm, Natalia Karpukhina, Delia S. Brauer,Julian R. Jones1, Robert V. Law, Robert G. Hill. Influence of strontium for calcium substitution in bioactive glasses on degradation, ion release and apatite formation. *J. R. Soc. Interface* 9, 880–889 (2012)

15. Esfahani, E. Salahi, A. Tayebifard, M.R. Rahimipour, M. Keyanpour. Influence of zinc incorporation on microstructure of hydroxyapatiteto characterize the effect of pH and calcination temperatures, *Journal of Asian Ceramic Societies* **2** : 248–252(2014)

16. A. Costescu, I. Pasuk, F. Ungureanu, A. Dinischiotua, M. Costachea, F. Huneaub, S. Galaupc, P. Le Coustumerb, D. Predoi. Physico-Chemical properties of nano-sized hexagonal hydroxyapatite powder synthesized by sol-gel, *Digest Journal of Nanomaterials and Biostructures* **5** (4) : 989-1000(2010)

17. Pierre Layrolle, Atsuo Ito, and Tetsuya Tateishi. Sol–Gel Synthesis of Amorphous Calcium Phosphate and Sintering into Microporous Hydroxyapatite, *Bioceramics, J. Am. Ceram. Soc.* **81** (6) : 1421–28 (1998)

18. S. Ramesha,n, K.L.Awb, R.Toloueic, M.Amiriyanc, C.Y.Tanb, M.Hamdia, J. Purbolaksonoa, M.A.Hassana, W.D.Teng. Sintering properties of hydroxyapatite powders prepared using different methods, Ceramics International 39 : 111–119 (2013)

19. Morteza Mehrjoo, Jafar Javadpour, Mohamad Ali Shokrgozar, Mehdi Farokhi, Sayfoddin Javadian, and Shahin Bonakdar. Effect of magnesium substitution on structural and biological properties of synthetic hydroxyapatite powder, Mater. Express 5 (1) : (2015)

20. S. Kobayashi, T. Murakoshi. Evaluation Of Mechanical Properties And Bioactivity Of Hydroxyapatite/β-Tricalcium Phosphate Composites, *Advanced Composite Materials* **23**(2) (2014)

21. Cristina Liana Popa, m. Albu, C. Bartha, A. Costescu, C. Luculescu, R. Trusca, S. Antohe. Structural characterization and optical properties of hydroxyapatite/collagen matrix, Romanian Reports in Physics 68 (3) : 1149–1158 (2016)

22. Christos G. Kontoyannis, Nikolaos C. Bouropoulos, Petros G. Koutsoukos, Raman spectroscopy: A tool for the quantitative analysis of mineral components of solid mixtures. The

case of calcium oxalate monohydrate and hydroxyapatite, Vibrational Spectroscopy 15 (1997) 53-60
23. Bengi Yilmaz, Zafer Evis, Raman Spectroscopy Investigation of Nano Hydroxyapatite Doped with Yttrium and Fluoride Ions, Spectroscopy Letters, 47:24–29, 2014
24. Geovana D. Webler a, Ana C.C. Correia b, Emiliano Barreto b, Eduardo J.S. Fonseca, Mg-doped biphasic calcium phosphate by a solid state reaction route: Characterization and evaluation of cytotoxicity, Materials Chemistry and Physics 162 (2015) 177e181
25. Guillaume Penel, Elodie Cau, Caroline Delfosse, Christian Rey, Pierre Hardouin, Joseph Jeanfils, Christophe Delecour, Jacques Lemaitre, Gérard Leroy, Raman Microspectrometry Studiesof Calcified Tissues and Related Biomaterials.Raman Studies of Calcium Phosphate Biomaterials, Dent. Med. Probl. 2003, 40, 1, 37–43
26. Ammar Z. Alshemary, M. Akram, Yi-Fan Goh, Usman Tariq, Faheem k. Butt, Ahmad Abdolahi, Rafaqat Hussain, Synthesis, characterization in vitro bioactivity and antimicrobial activity of magnesium and nickel mdoped silicate hydroxyapatite, ceramics international 41(2015) 11886-11898
27. P.Kanchana, Effect of magnesium on mechanical and bioactive properties of Biphasic calcium Phosphate
28. M. H. Salami, J. C. Heughebaert and G. H. Nancollas, "Crystal Growth of Calcium Phosphates in the Presence of Magnesium Ions." Langmuir, Vol. 1, No. 1, 1985, pp. 119-122
29. B.D. Cullity, Elements of X-ray Diffraction, second ed., Addison–Wesley Publishing Company, Massachusetts, 1978.
30. S. Samani, S. M. Hossainalipour, M. Tamizifar, H. R. Rezaie, In vitro antibacterial evaluation of sol–gel-derived Zn-, Ag-, and (Zn þ Ag)-doped hydroxyapatite coatings against methicillin-resistant Staphylococcus aureus, Journal Of Biomedical Materials Research A **101a**(1) (2013)
31. Z Evis, T J Webster. Nanosize hydroxyapatite: doping with various Ions, *Advances in Applied Ceramics* **110** (5) : 311-320 (2011)
32. O A Golovanova, R M Shlyapov, Sh K Amerkhanova, A S Uali and V A Vlasov. Effect of cations (Mg2+, Zn2+, Cd2+) on formation of the mineral phase in Ca(NO3) 2 -Mg(NO3) 2-Na2HPO4-H2O system, *Materials Science and Engineering* **81:** 1-6 (2015)
33. Mageda El Saied Hanafi1, Samira Mohamed Sallam2, Faten Adel Mohamed, Characterization of Hydroxyapatite Doped with Different Concentrations of Magnesium Ions, International Journal of Research Studies in Science, Engineering and Technology Volume 3, Issue 8, August 2016, PP 17-23
34. Laura floroian1, ion mihailescu2, felix sima3, gheorghe stanciu4, bogdan savu, evaluation of biocompatibility and bioactivity for polymethyl methacrylate – bioactive glass nanocomposite films obtained bymatrix assisted pulsed laser evaporation, u.p.b. Sci. Bull., series a, vol. 72, iss. 2, 2010
35. Hae Lin Jang , Guang Bin Zheng , Jungha Park , Hwan D. Kim , Hae-Ri Baek , Hye Kyoung Lee , Keunho Lee , Heung Nam Han , Choon-Ki Lee , Nathaniel S. Hwang , Jae Hyup Lee , Ki Tae Nam, In Vitro and In Vivo Evaluation of Whitlockite Biocompatibility: Comparative Study with Hydroxyapatite and β-Tricalcium Phosphate, Adv. Healthcare Mater., 5(1), 128-136 (2016)
36. Satoshi K.,Takuma Murakoshi, Characterization of mechanical properties and bioactivity of hydroxyapatite/β-tricalcium phosphate composites, Advance composite materials **23**(2) 2014
37. O. Kaygili • C. Tatar, The investigation of some physical properties and microstructure of Zn-doped hydroxyapatite bioceramics prepared by sol–gel method, J Sol-Gel Sci Technol (2012) 61:296–309

38. B. V. Jogiya, H. O. Jethava, K. P. Tank, V. R. Raviya, and M. J. Joshi, Impedance and modulus spectroscopic study of nano hydroxyapatite, AIP Conference Proceedings, Volume 1728, Issue 1(2016)

39. Kokubo T., Kushitani H., Sakka S., Kitsugi T.,Yamamuro T., J. Biomed. Mater. Res., 24/6, (1990), 721.

40. Sunil Prasad, Vikas Kumar Vyas, Kumari Deepa Mani,Md. Ershad, Ram Pyare. Preparation In-Vitro Bioactivity And Mechanical Properties of Reinforced 45S5 Bioglass Composite With HA-ZrO2 Powders. Orient. J. Chem., 33(3) : 1286-1296 (2017).

41. R. Zia , M. Riaz, N. Nasir, F. Saleemi , Z. Kayani, S. Anjum, F. Bashir, T. Hussain. Bioactivity analysis of theTa(V)dopedSiO2–CaO–Na2O–P2O5 ceramics prepared by solid state sintering method. Progress in Natural Science : Materials International 26 : 41 – 48 (2016)

42. Anusuya Nagaraj, Suja Samiappan. Presentation of antibacterial and therapeutic anti-inflammatory potentials to hydroxyapatite via biomimetic with azadirachta indica: An in vitro anti-inflammatory assessment in contradiction of LPS-induced stress in RAW 264.7 cells. *Frontiers in Microbiology* **10**(1757) : 1 – 15

43 A. Elfalaky, H. Hashem, T. Mohamed. Bone-like Material, Synthesis, Optimization and Characterization. *Nanosci. Nanoeng.* 2 10-16 (2014).

Figures

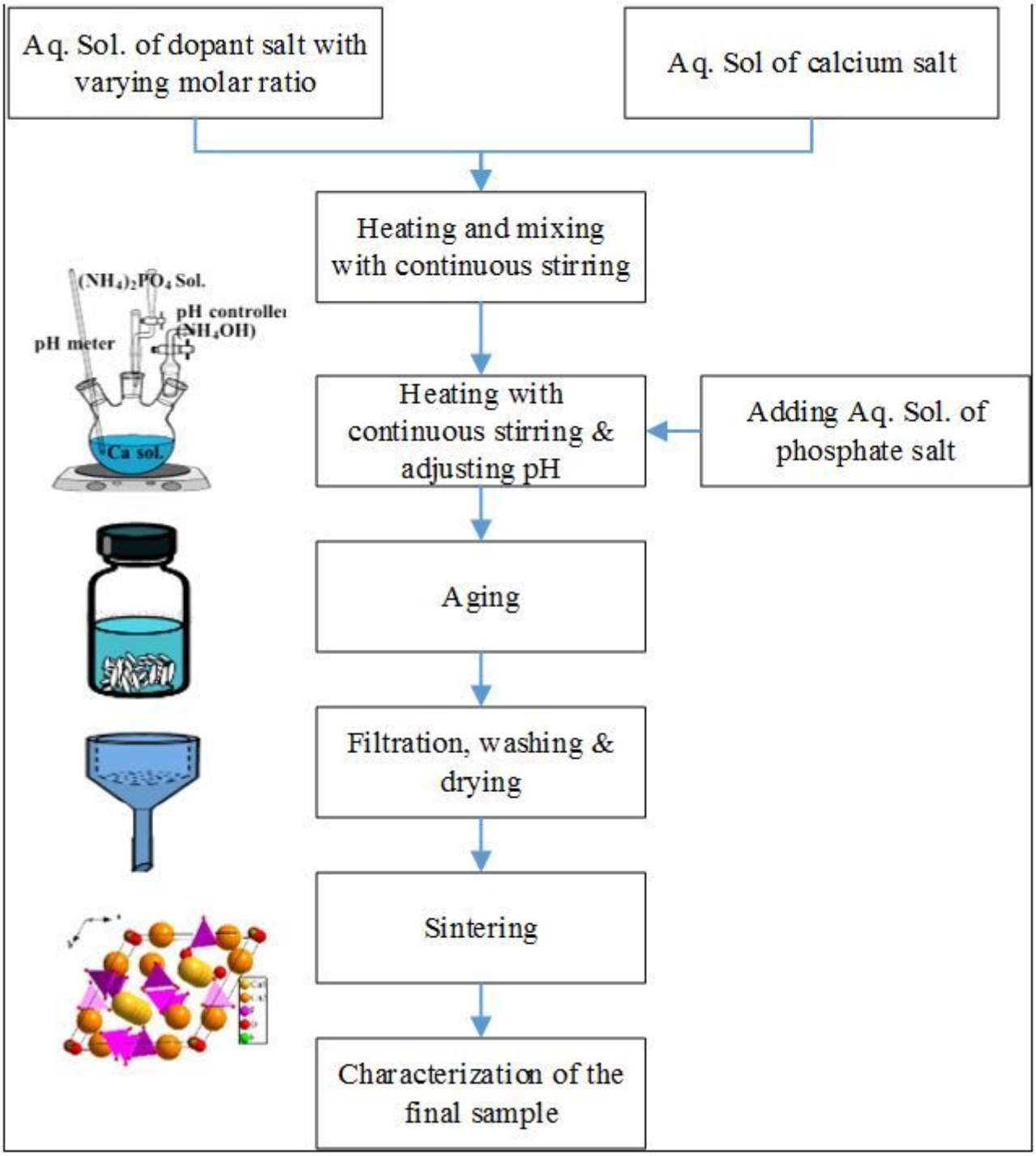

Figure 1

Schematic for Synthesis of the Samples

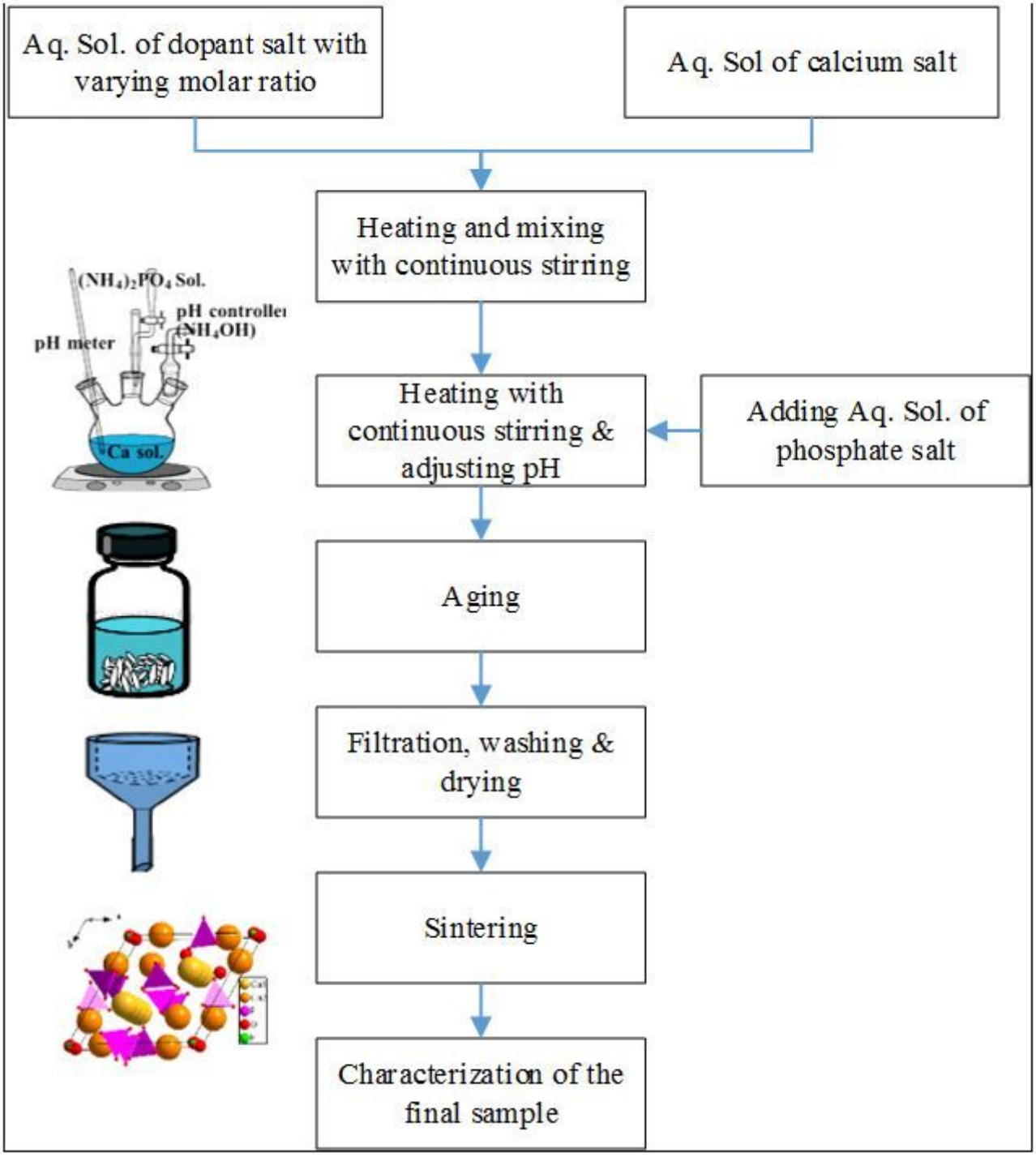

Figure 1

Schematic for Synthesis of the Samples

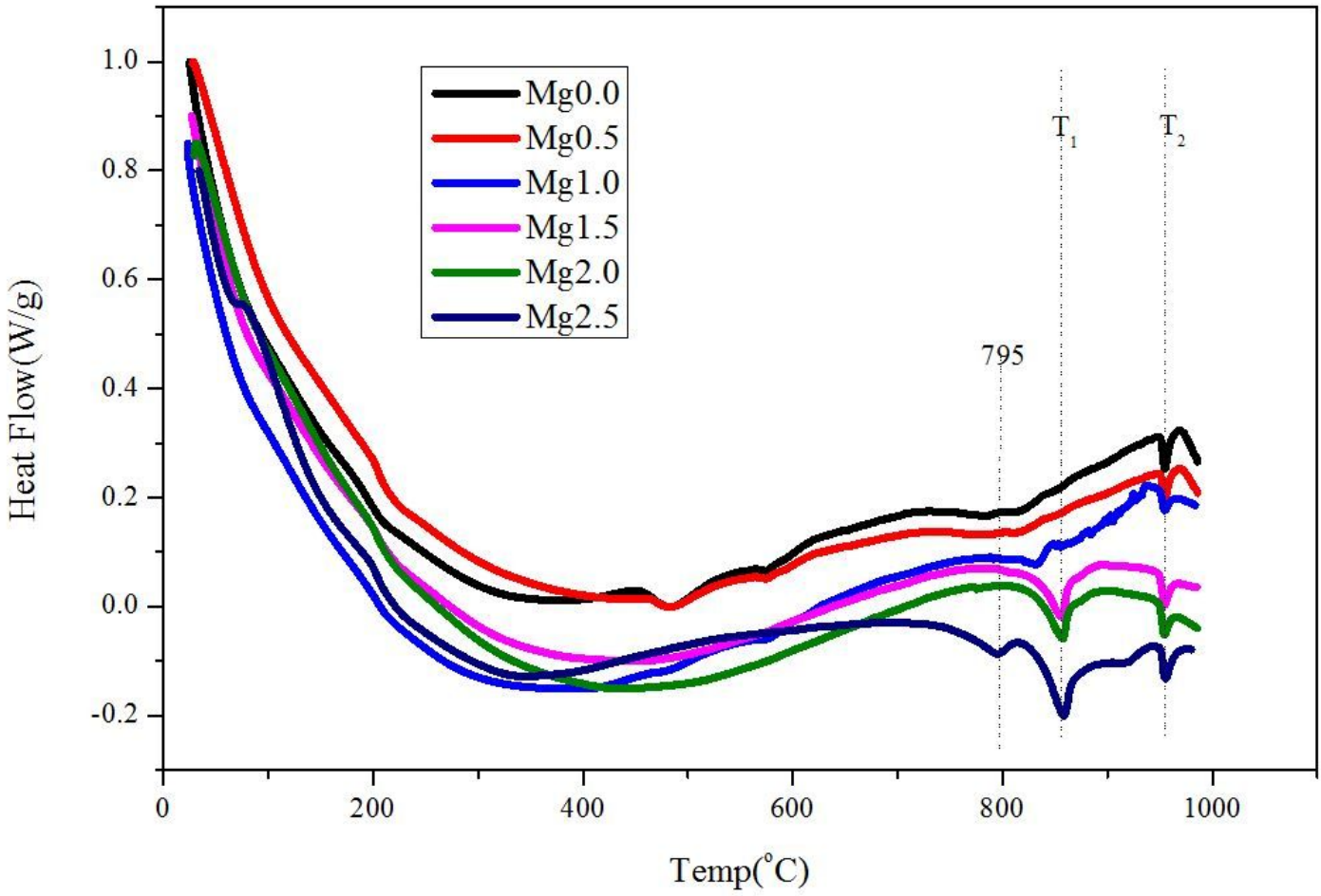

Figure 2

DSC curves for undoped and Mg-doped samples

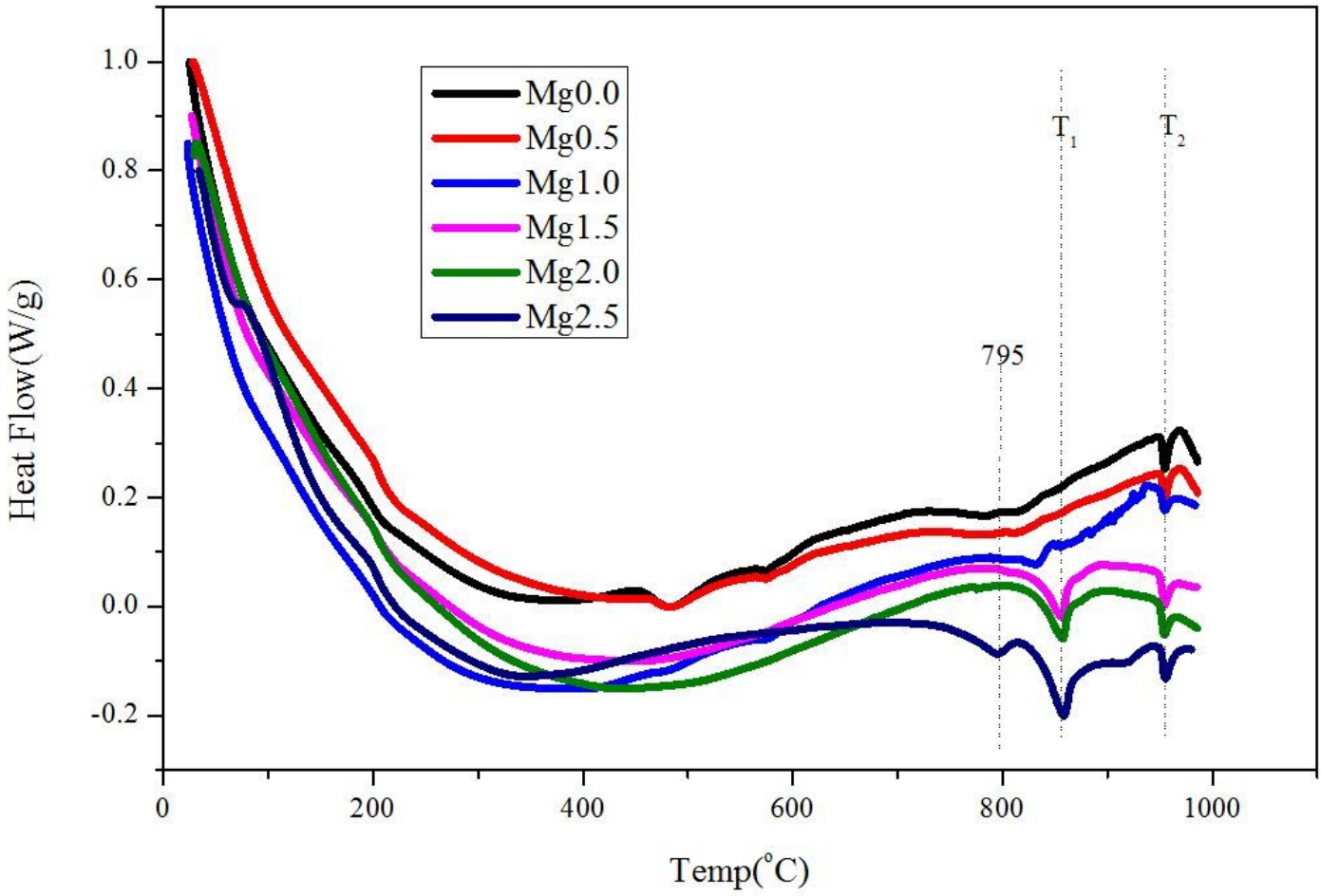

Figure 2

DSC curves for undoped and Mg-doped samples

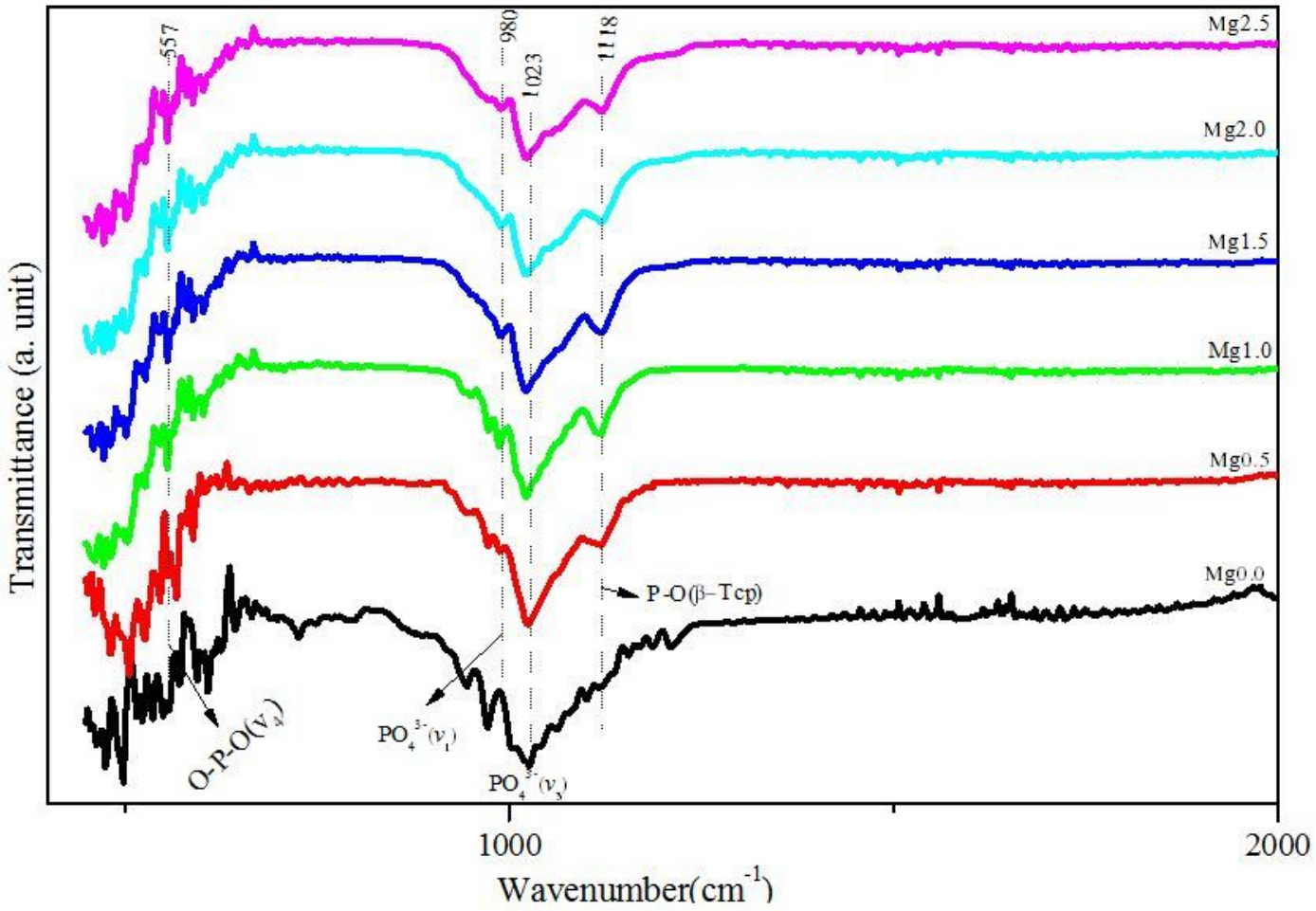

Figure 3

FTIR spectra of undoped and Mg doped hydroxyapatite

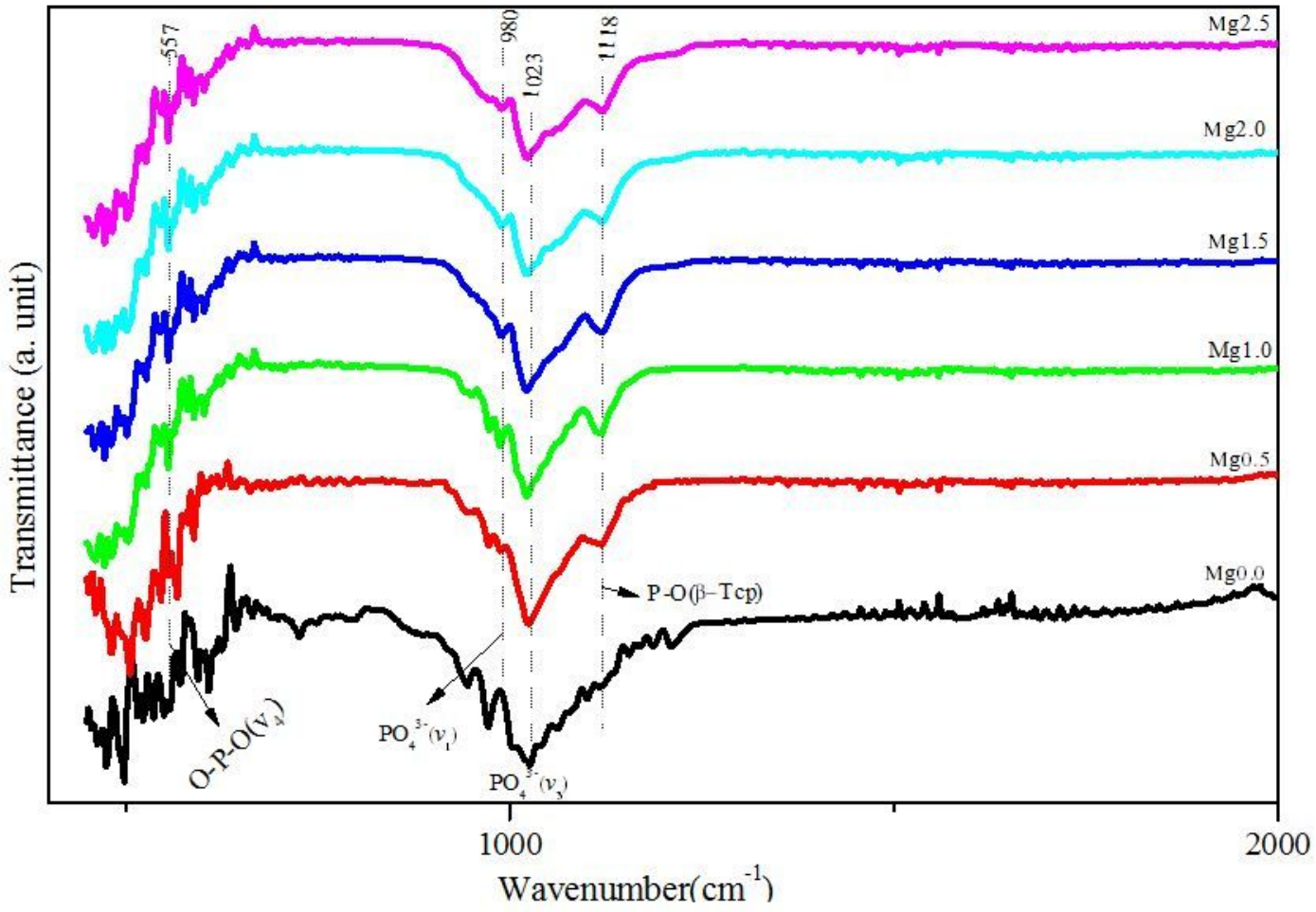

Figure 3

FTIR spectra of undoped and Mg doped hydroxyapatite

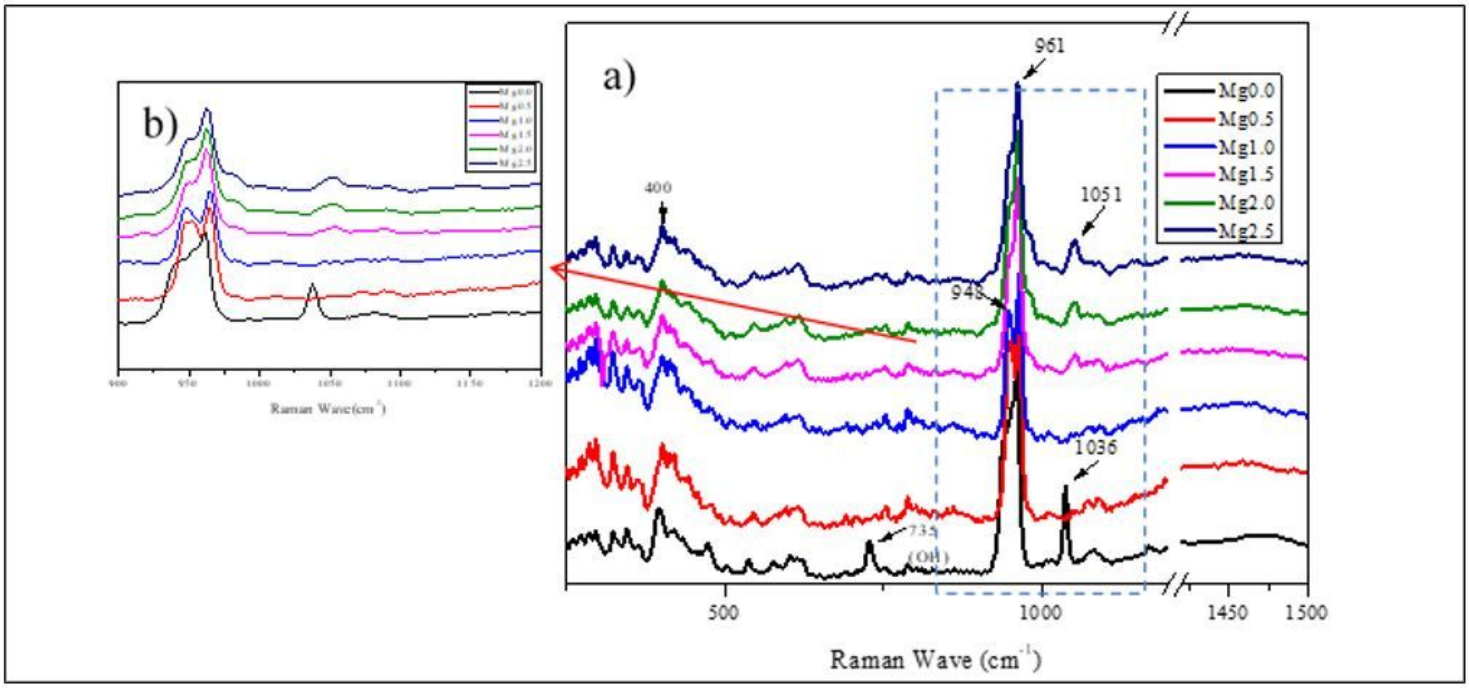

Figure 4

a)Raman Spectra of undoped and Mg doped samples b) Magnified view of a)

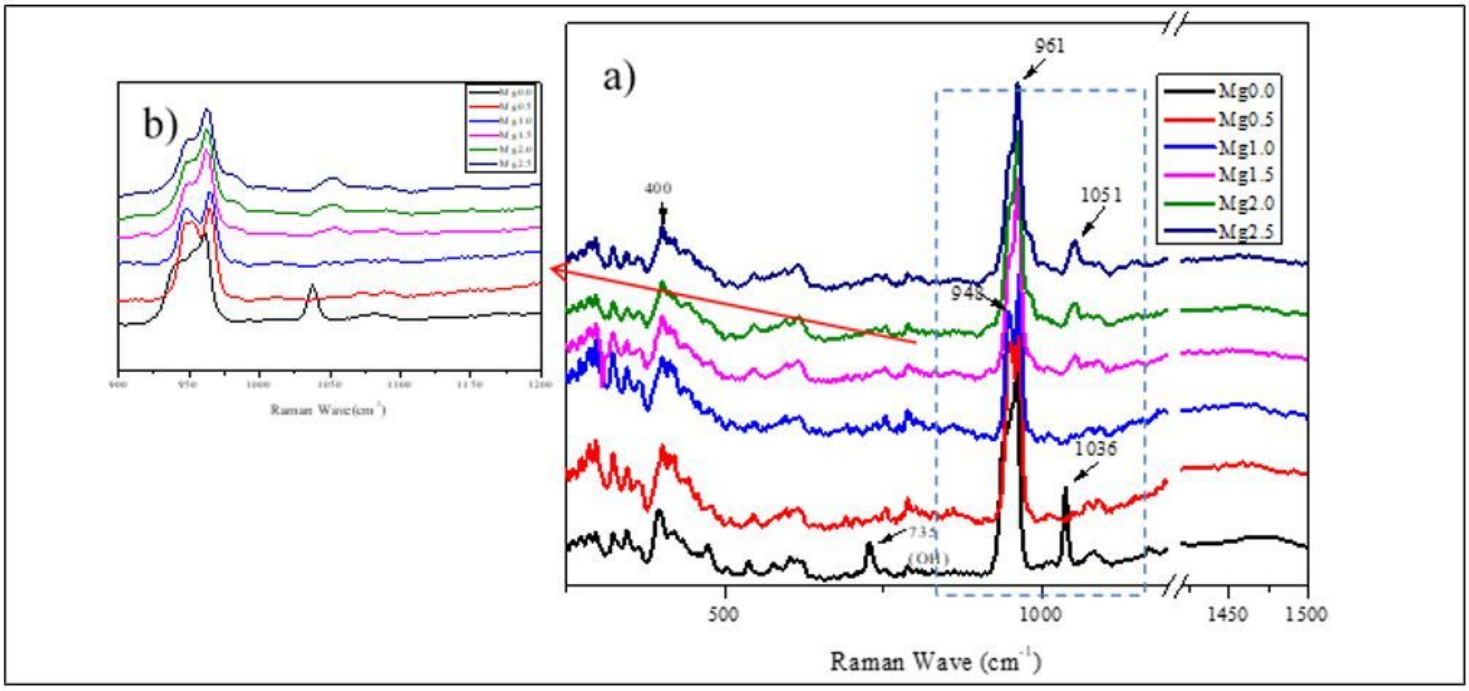

Figure 4

a)Raman Spectra of undoped and Mg doped samples b) Magnified view of a)

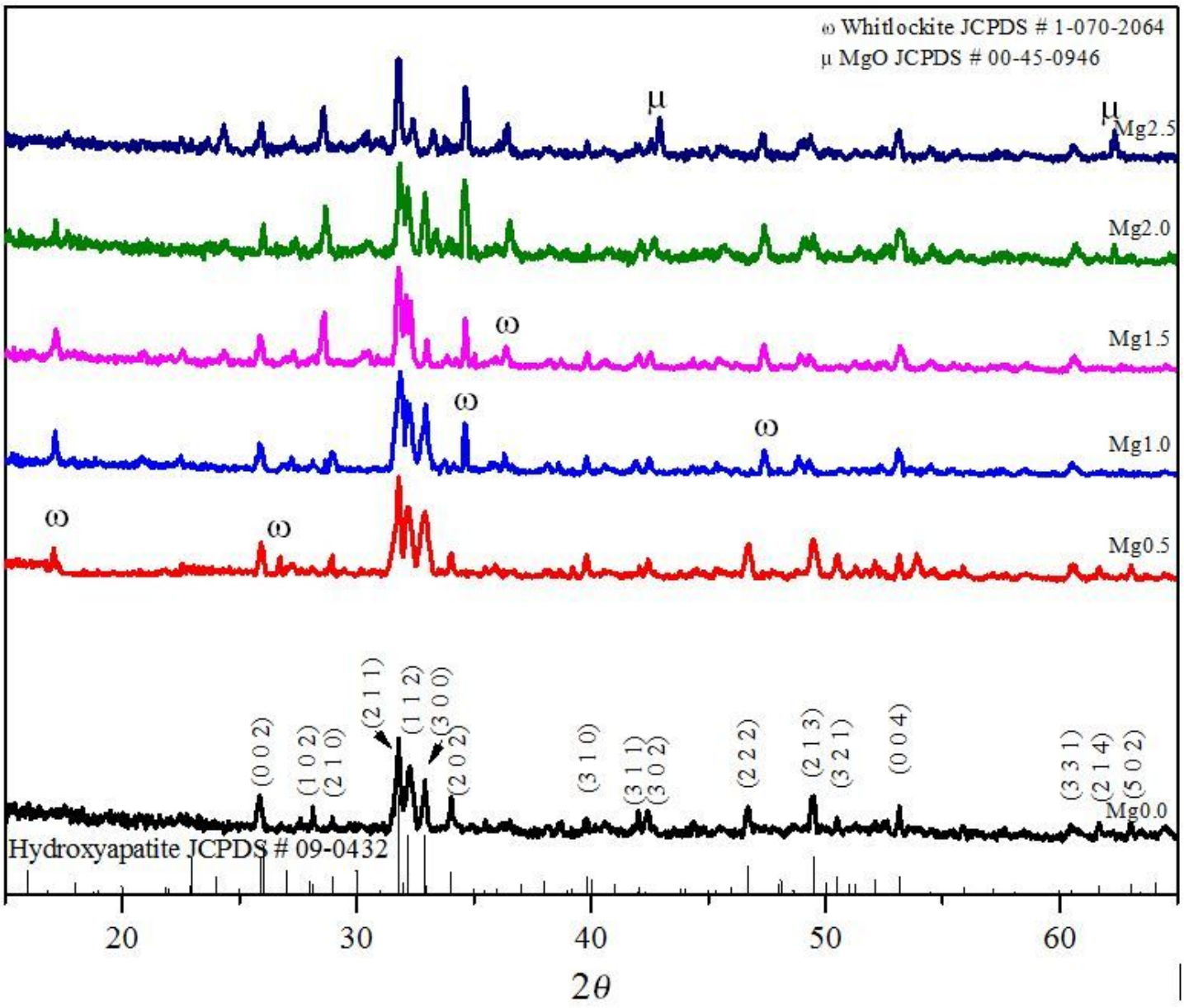

Figure 5

XRD pattern of undoped and Mg(0 – 2.5mol%)

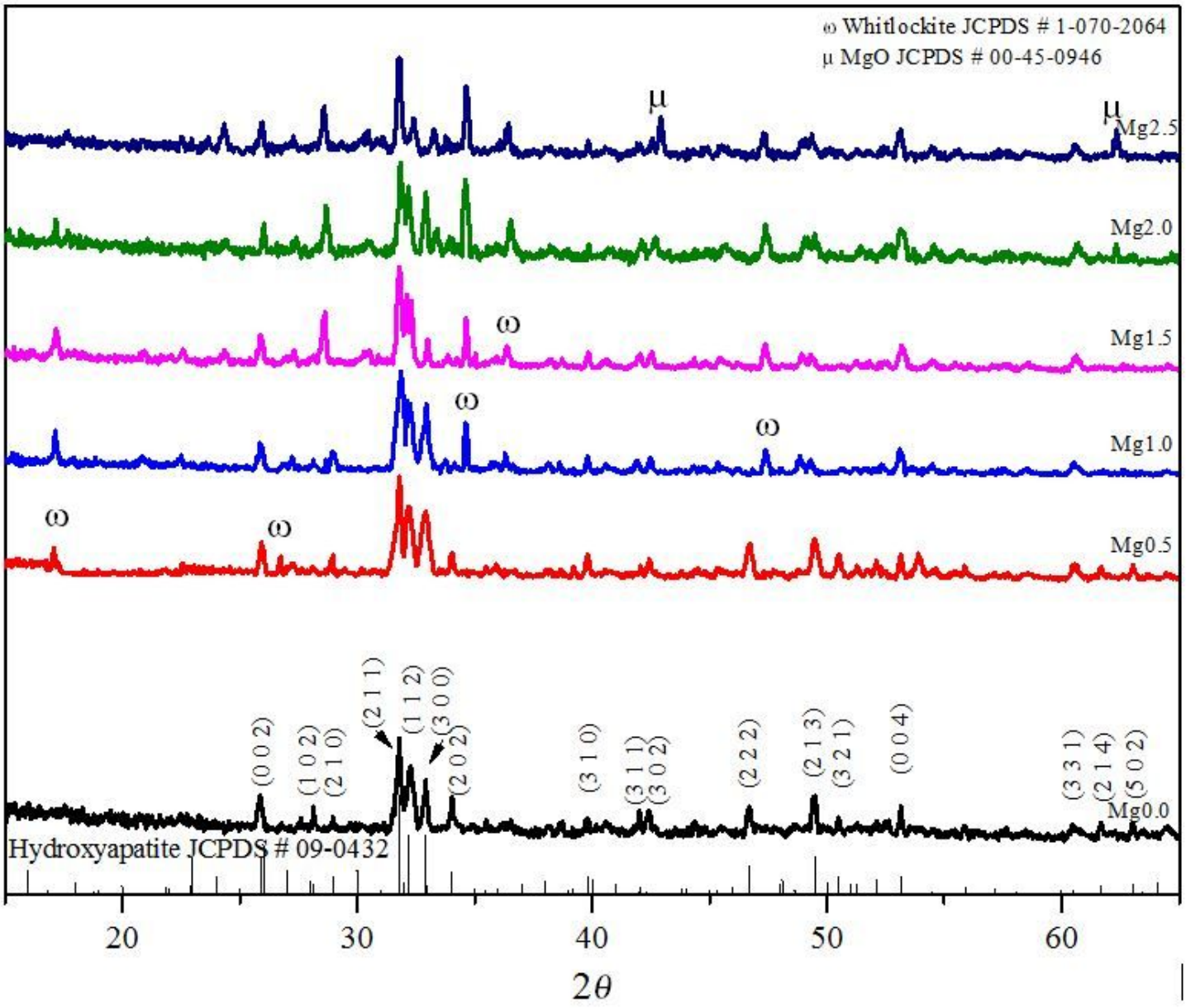

Figure 5

XRD pattern of undoped and Mg(0 – 2.5mol%)

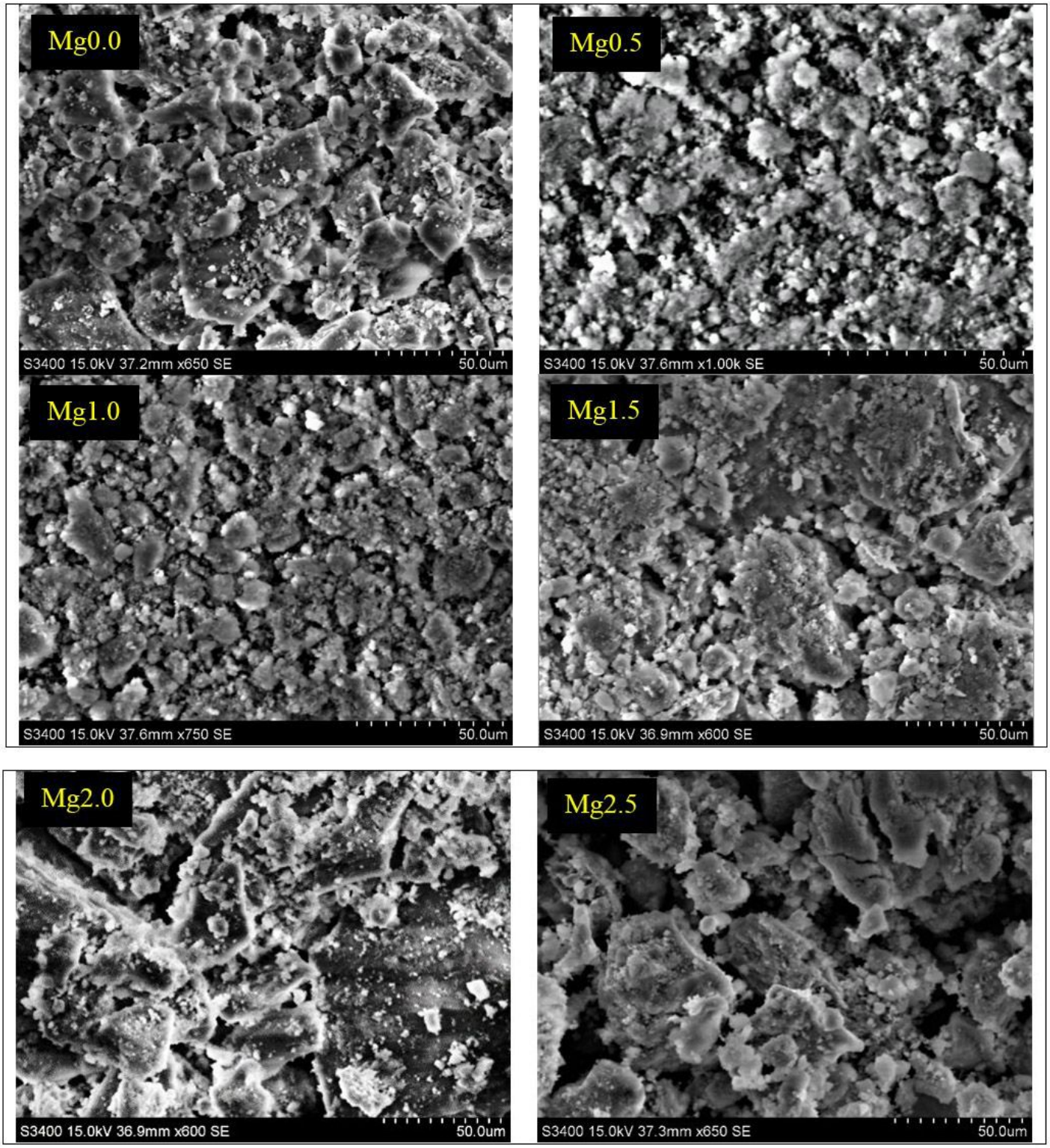

Figure 6

SEM micrograph of Mg doped samples

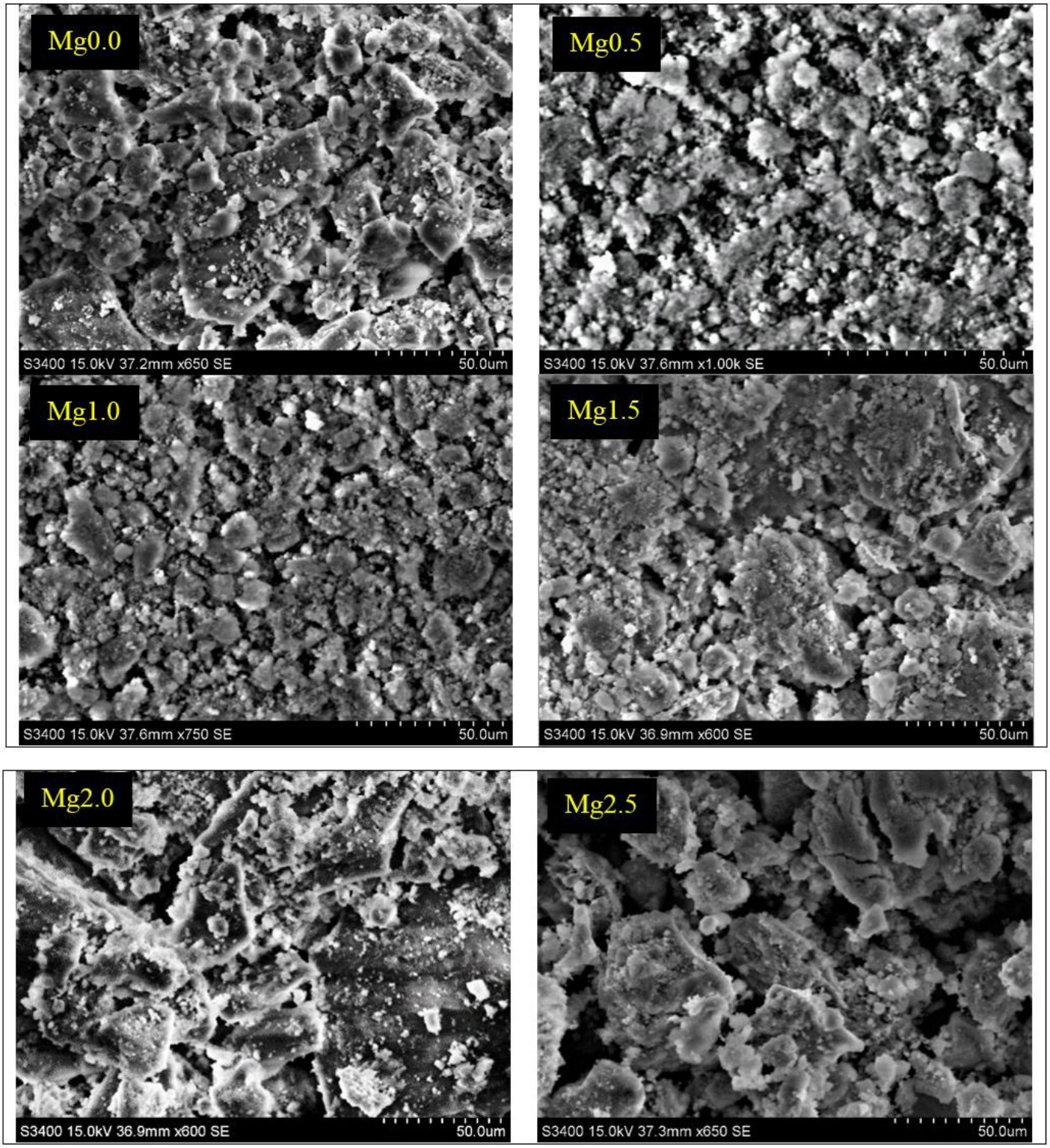

Figure 6

SEM micrograph of Mg doped samples

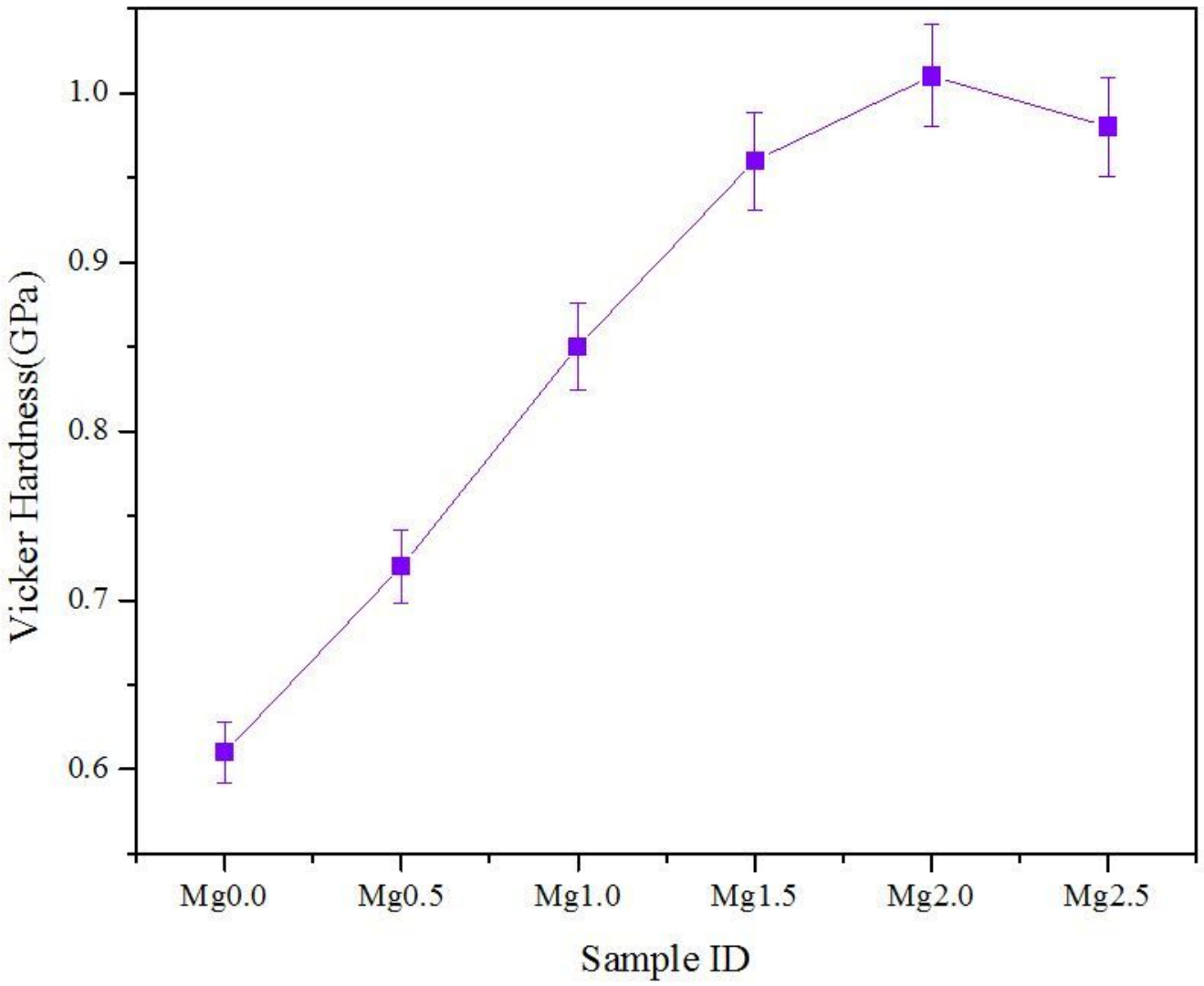

Figure 7

Vicker hardness of undoped and Mg doped samples

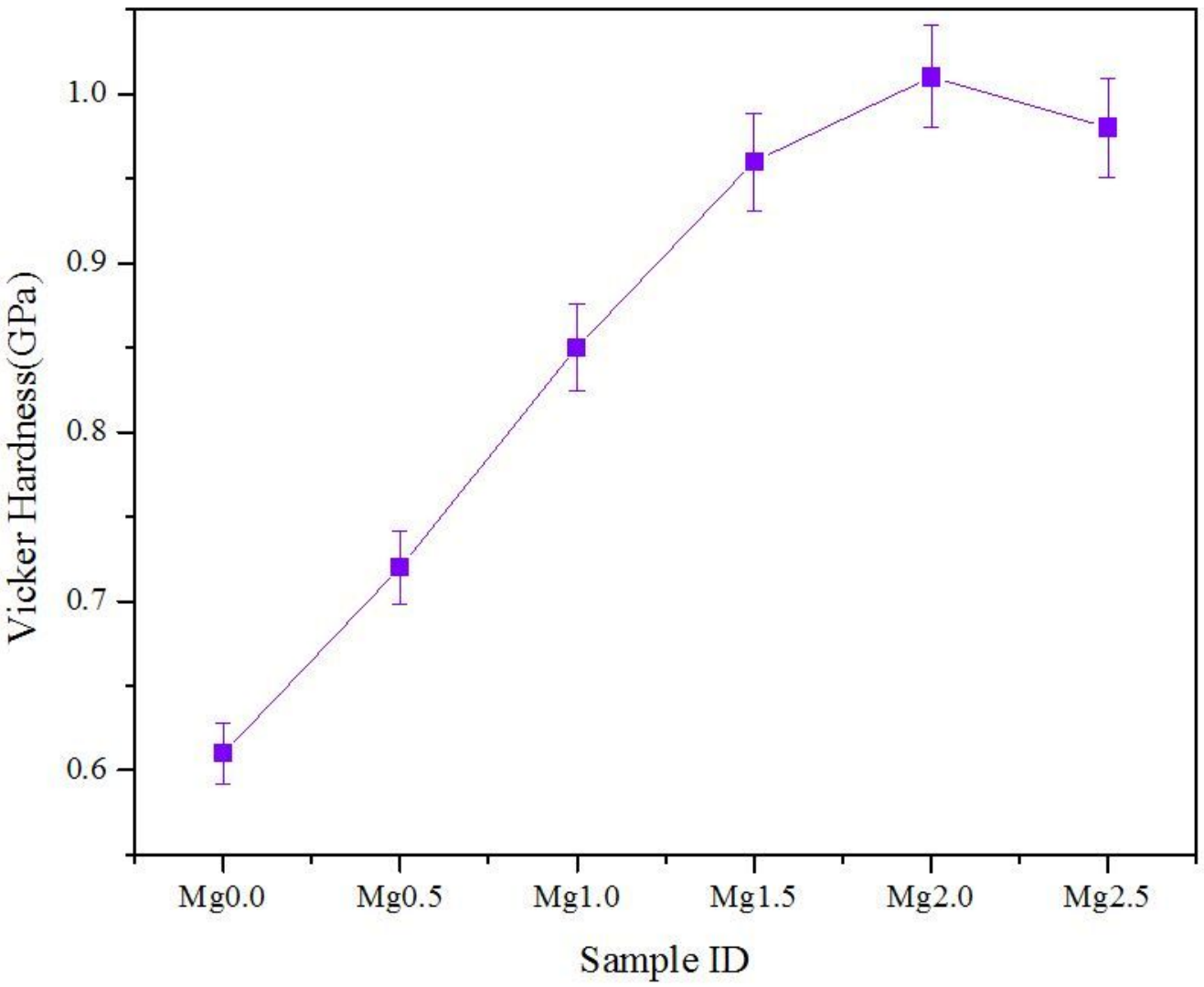

Figure 7

Vicker hardness of undoped and Mg doped samples

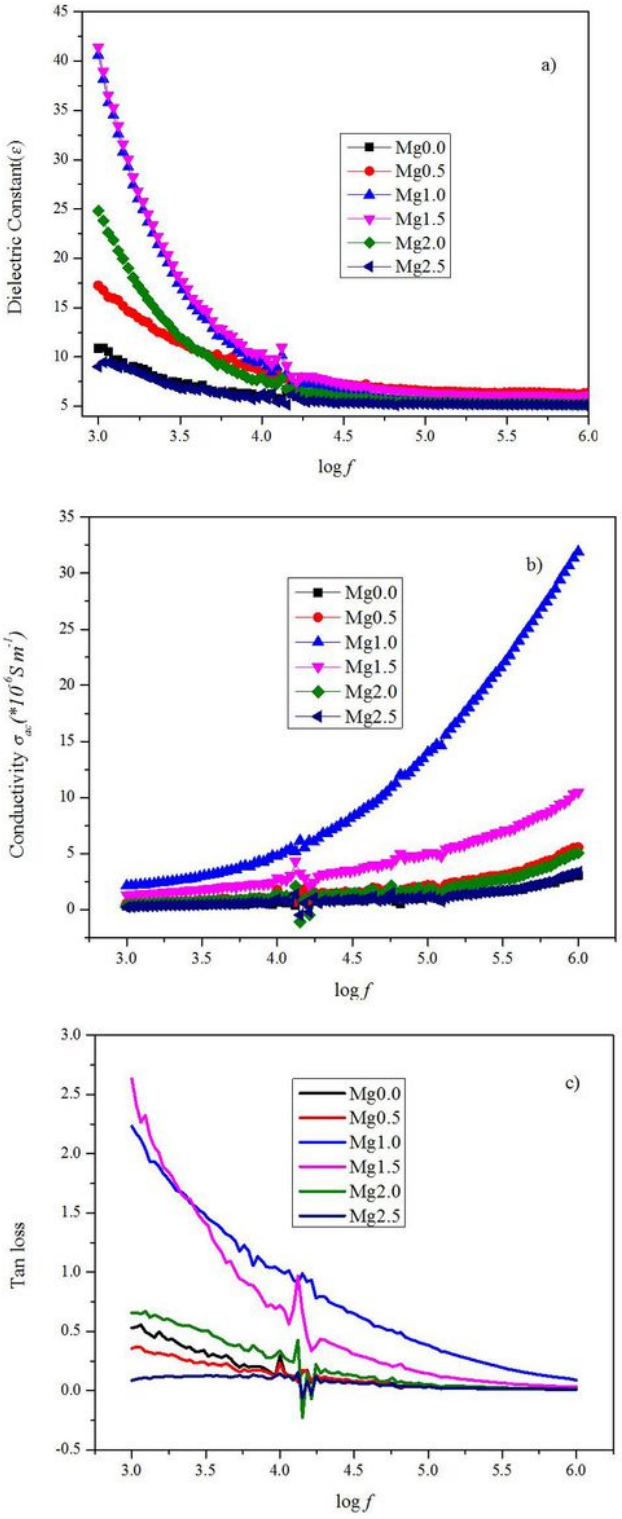

Figure 8

Relative Permativity, AC conductivity and Tangent Loss as a function of frequency for Mgx content (0 ≤ x ≤ 2.5 mol%).

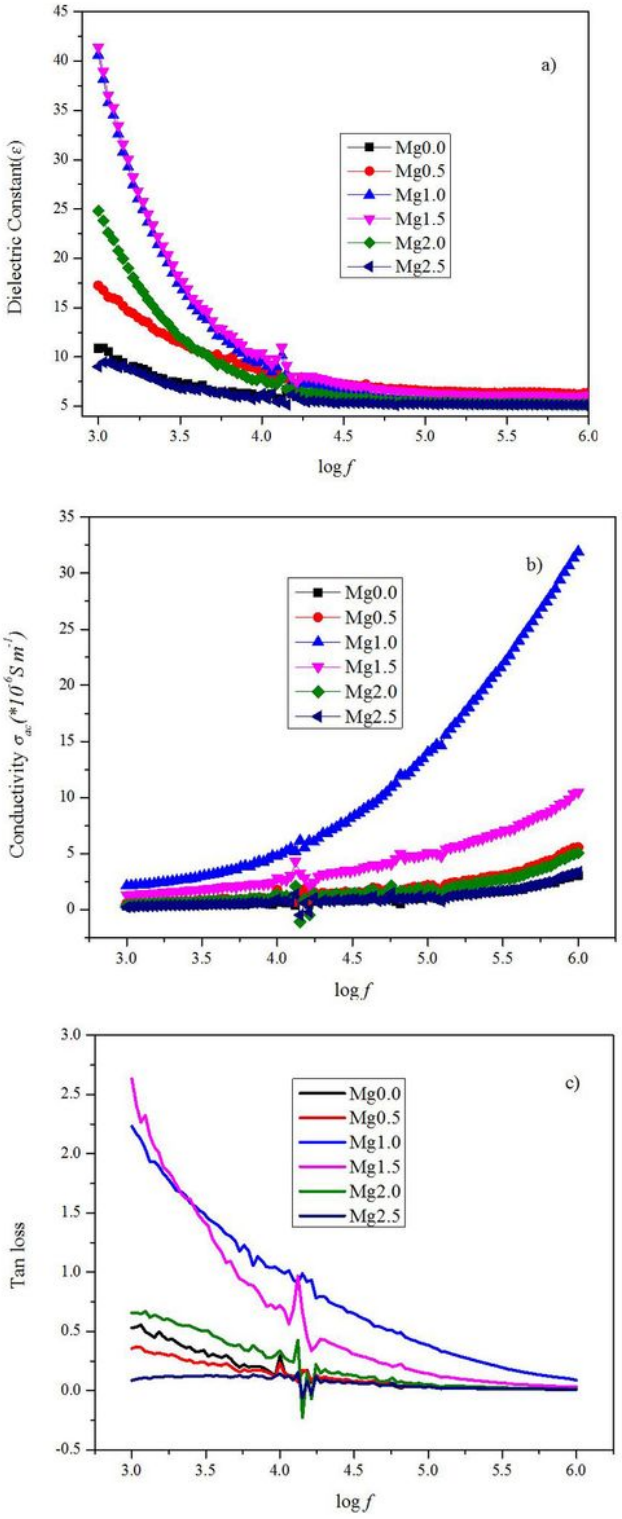

Figure 8

Relative Permativity, AC conductivity and Tangent Loss as a function of frequency for Mgx content (0 ≤ x ≤ 2.5 mol%).

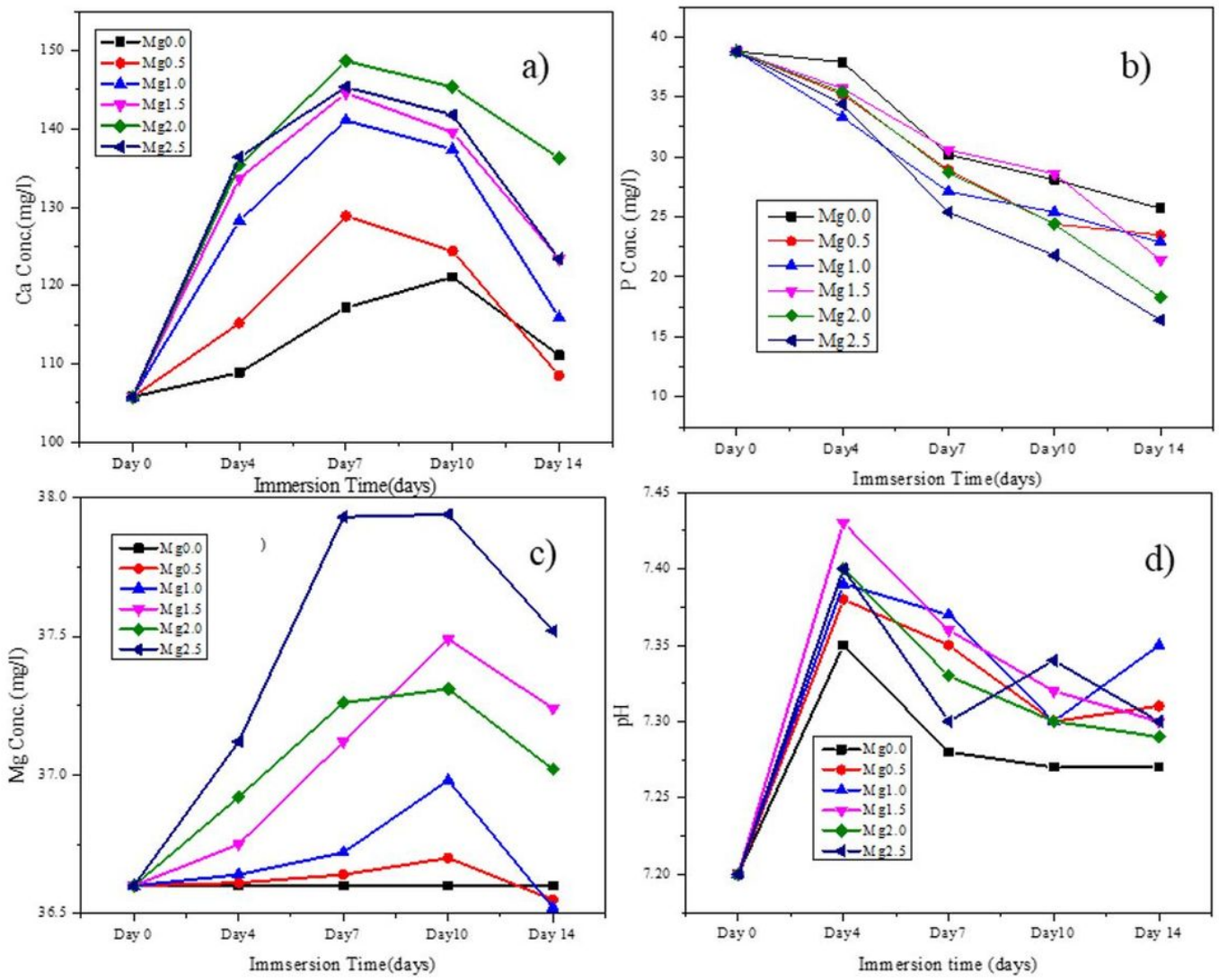

Figure 9

Ca Concentration(a), P concentration(b) Mg concentration(c) and Variation of pH(d) in SBF Sol. For 14 days

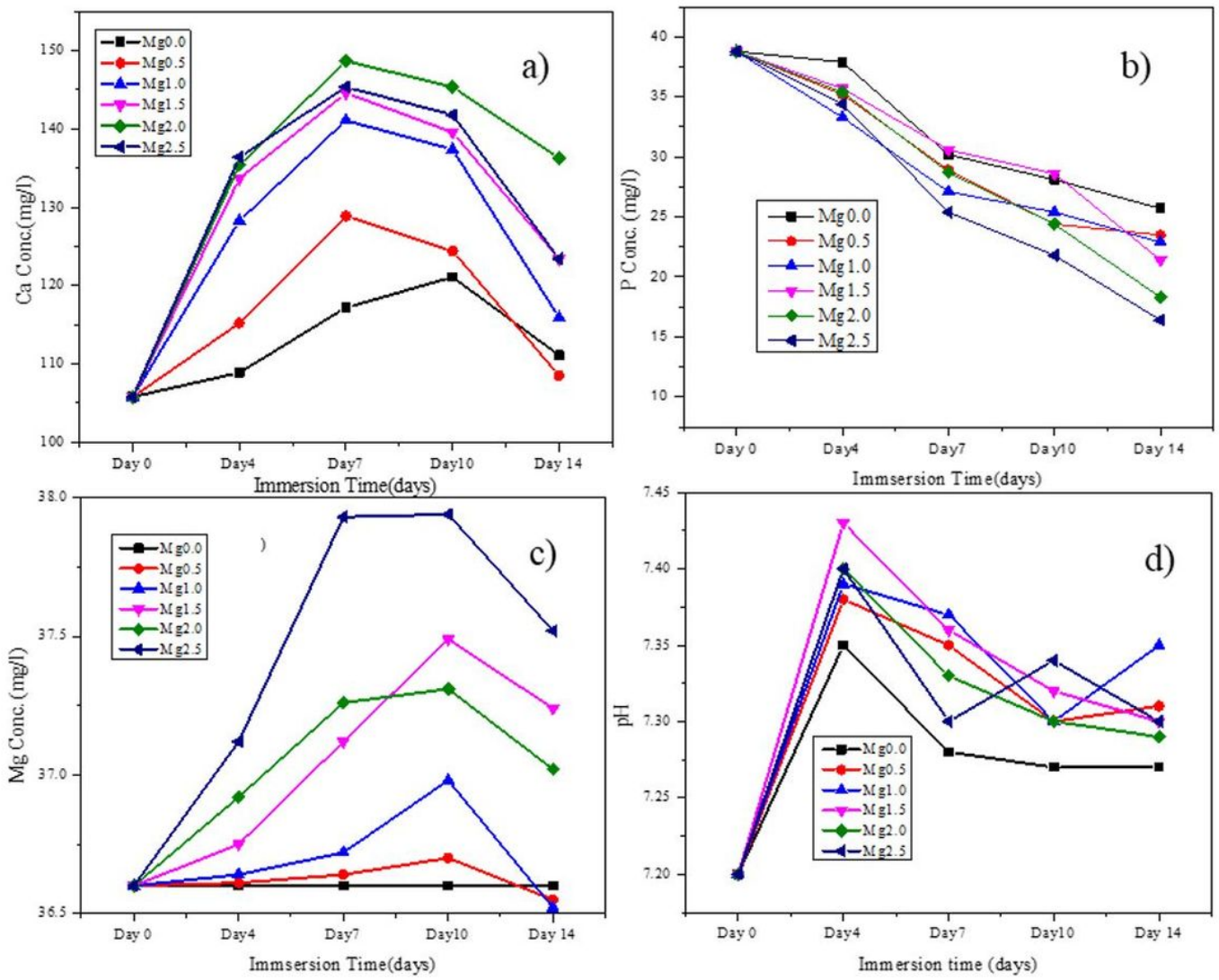

Figure 9

Ca Concentration(a), P concentration(b) Mg concentration(c) and Variation of pH(d) in SBF Sol. For 14 days

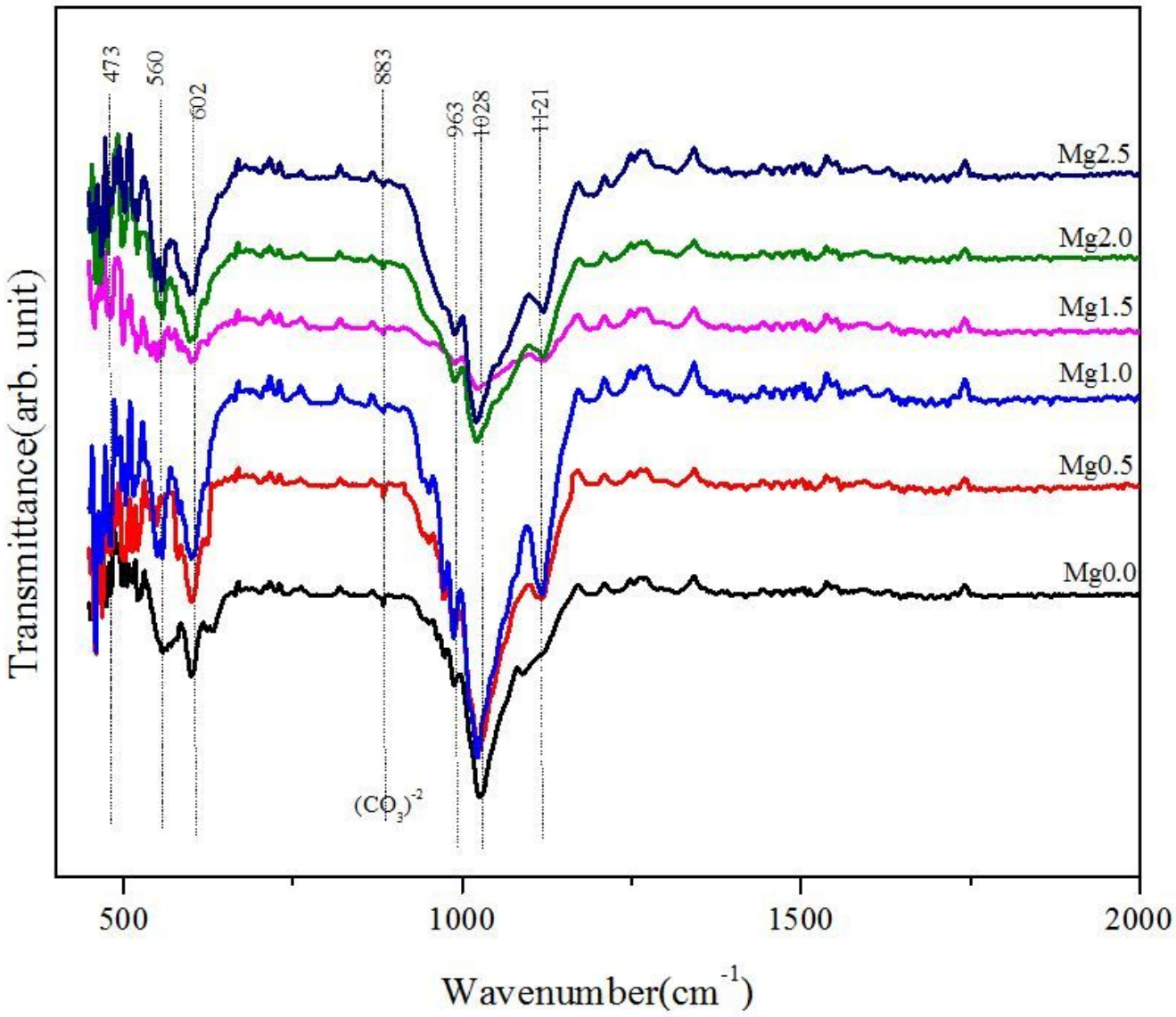

Figure 10

FTIR of undoped and Mg-doped samples after immersion in SBF Sol.

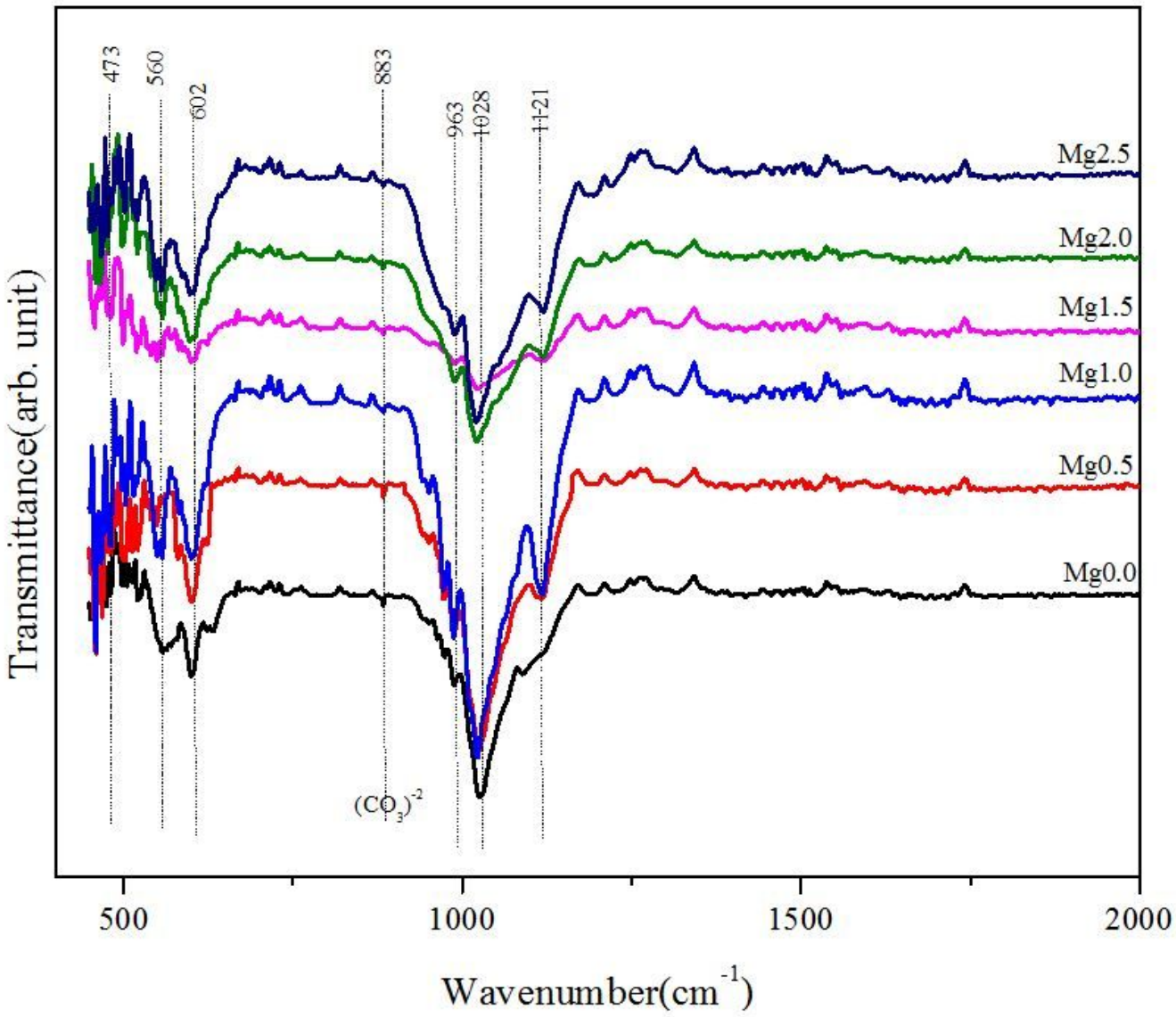

Figure 10

FTIR of undoped and Mg-doped samples after immersion in SBF Sol.

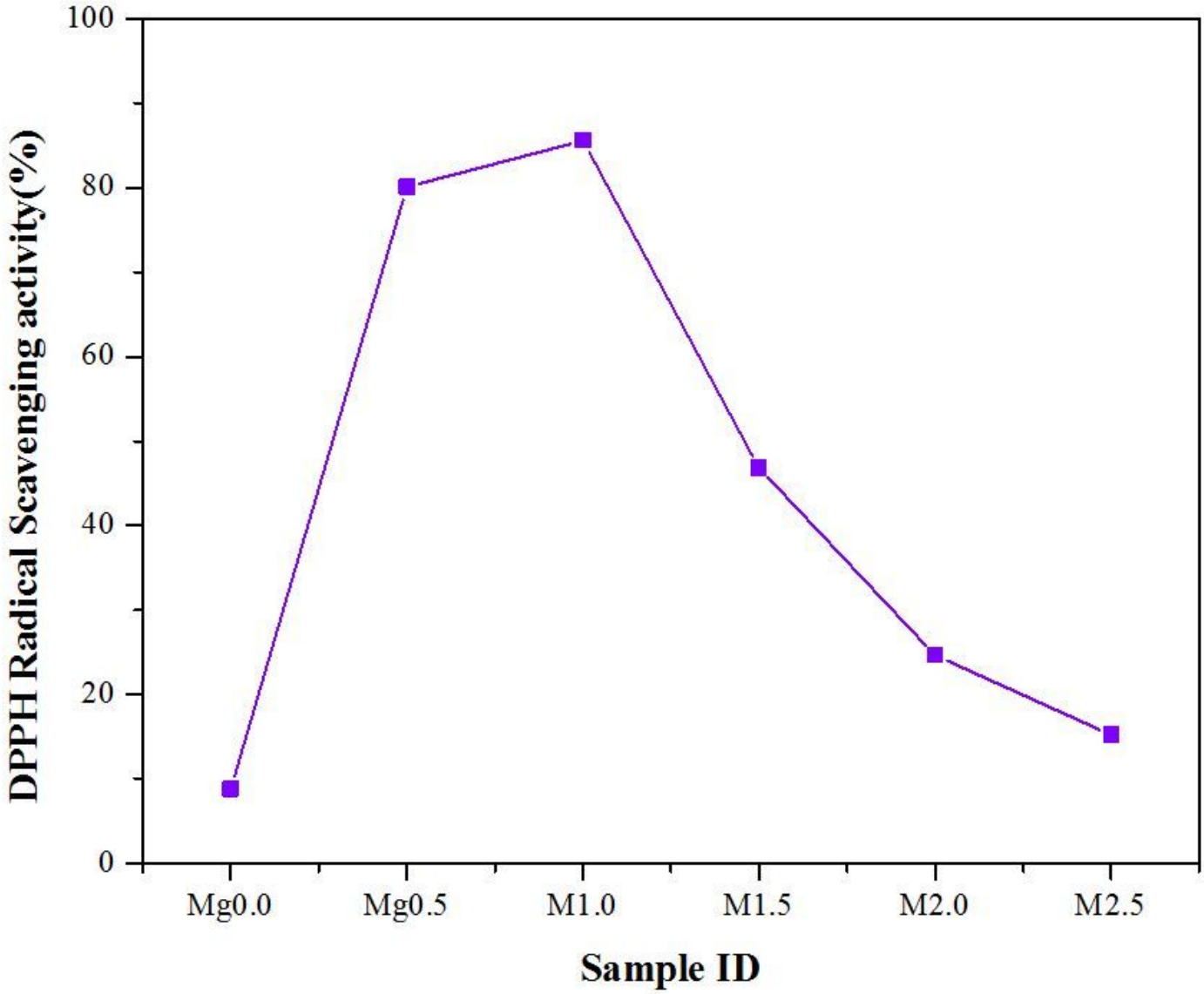

Figure 11

Antioxidant activity of samples for Mgx content ($0 \leq x \leq 2.5$ mol%).

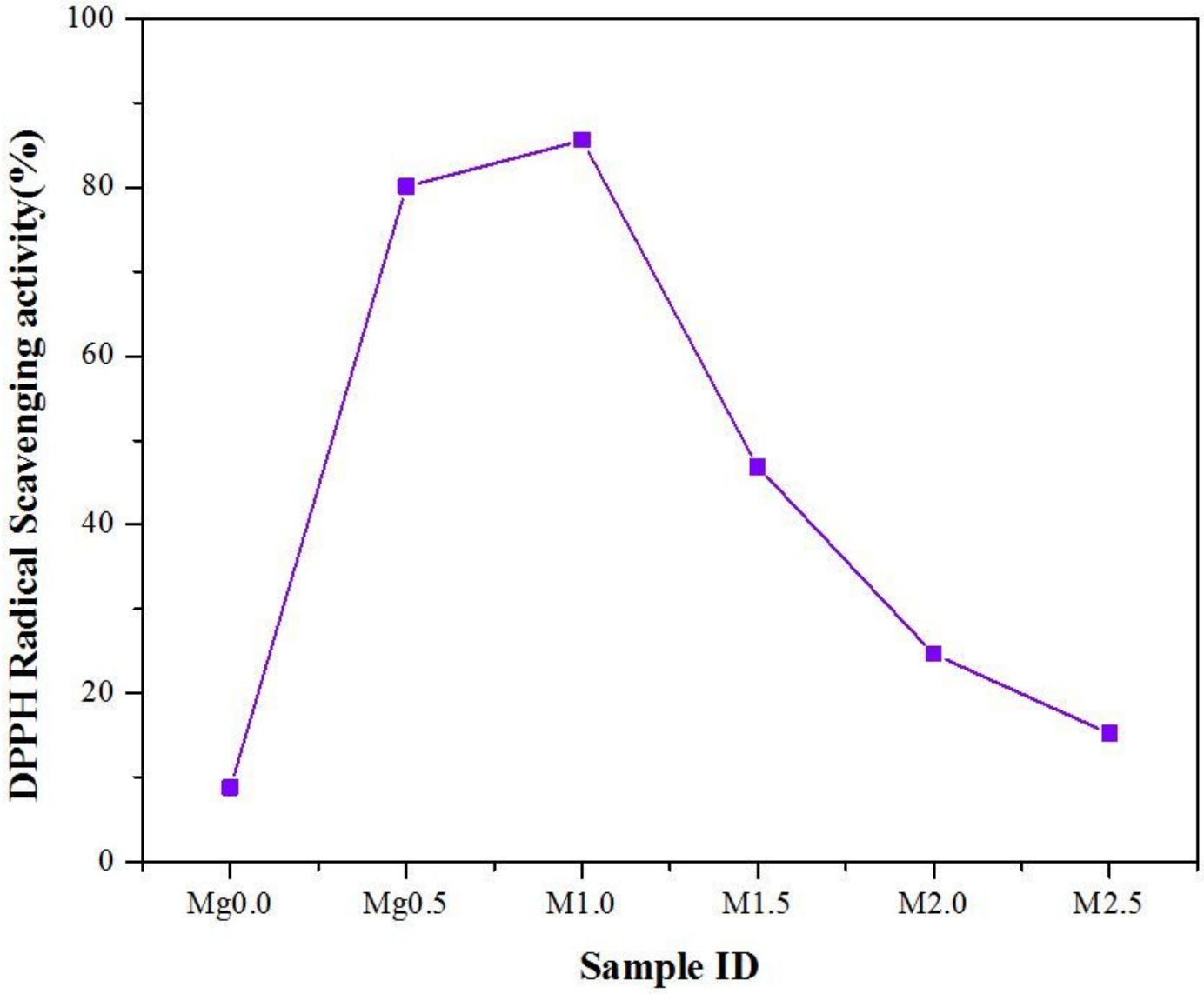

Figure 11

Antioxidant activity of samples for Mgx content ($0 \leq x \leq 2.5$ mol%).